The Quantum Szilard Engine: Interactions, Impurities and Dynamics

Master Thesis in Physics

Mikael Nilsson Tengstrand

LUND UNIVERSITY

Division of Mathematical Physics, LTH, September 2016

Abstract

In this thesis, different aspects of the quantum Szilard engine are studied using the configuration interaction method. The engine is modelled as a one-dimensional infinite well.

The effects of a contact-interaction are examined and it is found that attractive contact-interactions can improve the work output at certain temperatures of an engine that has bosons as a working medium.

The role of impurities in the engine is investigated and found to have a large impact on the low-temperature behaviour of the engine.

Dynamics of a single-particle engine are considered in order to identify finite-speed effects in the engine's cycle.

Acknowledgements

I would like to thank Stephanie Reimann for giving me the opportunity to do this thesis and for welcoming me into her research group. I am grateful for the discussions we have had and all the guidance she has provided.

I would also like to thank Jakob Bengtsson for sharing his knowledge when we together found out about the important role of interactions in the bosonic Szilard engine. Another big thanks to him for always being able to provide excellent explanations to all of my questions and for his configuration interaction method library which I have used during this thesis.

Finally, a big thanks to Peter Samuelsson for examining my thesis.

Contents

Chapter 1

Introduction

For almost a century, the Szilard engine has acted as a tangible way to study the role of information in physics. The idea of an engine driven entirely by information was conceived by Leo Szilard in 1929 [1], and has been studied in many different ways ever since [2–10]. The simplest instance of the Szilard engine consists of a single particle in a box connected to a heat bath at a constant temperature. The box is then divided into two halves with an impenetrable partition, and the position of the particle is measured. Based on the outcome of the measurement an external load can be attached to the system and work can be extracted through isothermal expansion.

The ideas of the Szilard engine can also be brought into the quantum realm. While the work associated with the insertion and removal processes may be assumed to be zero for the classical engine, this is not the case for the quantum one. For a quantum Szilard engine, inserting or removing a partition—even an arbitrarily thin one—changes the system and shifts the energy levels, which implies that these processes must be associated with non-zero work. Additionally, we have at the quantum level different particle statistics which govern the behaviour of the engine [4]. The Szilard engine is described more thoroughly in chapter 2.

Classical information to work conversions with schemes similar to that of the Szilard engine have been realized experimentally [11, 12], but so far no quantum versions have been made. The quantum Szilard engine is often treated in a highly idealized way, so for this master thesis I have studied the engine under less ideal circumstances. The things that I have looked at are how interactions and impurities affect the work output of the engine, as well as some properties of the processes of the engine when the steps are not carried out quasi-statically. Much of the work of this thesis has been carried out numerically, using the configuration interaction method.

The history and theory of the Szilard engine are described in chapter 2. Short reviews of some of the most important theoretical concepts are given in chapter 3, along with an outline of the method used to obtain the results in chapters 4 and 5. Chapter 4 contains results for the quantum Szilard engine when its working medium consists of interacting particles. Irregularities in the confining potential—referred to as impurities throughout this thesis—are treated in chapter 5 and the dynamics of the engine in chapter 6. The thesis is concluded in chapter 7.

Chapter 2

The Szilard Engine

The Szilard engine is the central topic of this thesis, and this chapter is dedicated to provide theory for the results in the upcoming chapters. Before this can be done, however, Maxwell's demon has to be introduced. This chapter gives a brief overview of the historical background relevant to the Szilard engine followed by sections analysing both its classical and quantum versions in more detail.

2.1 Background

2.1.1 Maxwell's Demon

What would later be known as Maxwell's demon was first introduced in 1867 in a letter from James Clerk Maxwell to Scottish physicist Peter Tait [2]. In this letter, Maxwell describes a thought experiment with a gas in thermal equilibrium which is divided into two equally large sections by a wall with a small hole covered by a shutter that can be opened and closed frictionlessly.

Within the gas, Maxwell envisioned a small intelligent being—today known as Maxwell's demon—with the ability to distinguish between the particles of the gas, measuring their positions and momenta. Using this information in conjunction with the shutter, the demon was thought to be able to allow particles faster than the average particle to pass from one side, while simultaneously disallowing particles slower than average to pass in this direction. In the opposite direction, the demon would let only slower than average particles pass while disallowing the fast ones. This sorting process creates a temperature difference in the gas, without having expended any work (though it is important to note that the demon has to gain some amount of information to perform this sorting scheme), which is in violation of the second

law of thermodynamics. Maxwell used this thought experiment to argue that the second law is not an absolute law, but rather a statistical principle [2].

2.1.2 Szilard's Engine

Maxwell's demon managed to avoid serious scrutiny for the first couple of decades of its life. It was not until 1929, when Leo Szilard presented an engine assisted by such an intelligent being [1], that the demon would see renewed interest.

The Szilard engine is a special kind of engine driven by information that utilizes only a single heat bath of some constant temperature, which is against the Kelvin-Planck formulation of the second law of thermodynamics [2].

A simple version of the Szilard engine consists of a single particle assumed to obey the ideal gas law which is initially confined to some volume. The cycle of the engine has four steps: insertion, measurement, expansion and removal, see Fig. 2.1. In the first step, a thin adiabatic partition is inserted which divides the volume into two new equally sized volumes. Classically, this process is assumed to do no work, and the particle is now in either of the two volumes with equal probability. In the second step, a measurement is made by the demon and the particle is found on one side. The information about the position of the particle is stored by the demon so that an external load can be attached to the system, depending on which side the particle is found. In the third step the system is expanded quasi-statically and isothermally while being connected to a constant temperature heat bath. This expansion is done until the partition reaches the end of the container and results in work

$$W = k_B T \int_{V/2}^{V} \frac{dV'}{V'} = k_B T \ln 2 \tag{2.1}$$

being transferred to the external load. In expression (2.1), k_B is Boltzmann's constant, T the temperature of the heat bath and V the total volume of the box. The work (2.1) is taken as heat Q from the heat bath. In the fourth and last step, the partition is removed—again without any work cost or gain—along with the external load. This step brings the engine back to its initial state again, see Fig. 2.1 for an illustration of the whole cycle.

In total, due to conservation of energy, heat Q has been lost by the heat bath and work $W = Q = k_B T \ln 2$ has been gained by the external load. Since the system has been reset to its initial state, the entropy change of the single particle system for the whole cycle is zero. For the heat bath the entropy change is $\Delta S = -Q/T = -k_B \ln 2$, if Q is the heat absorbed *by* the system. This decrease in entropy clearly violates the second law of thermodynamics, for the second law to hold there must be an

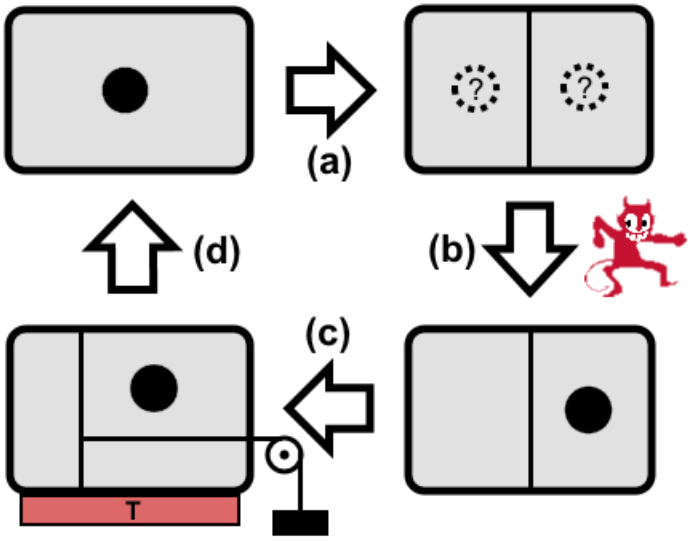

Figure 2.1: The cycle of the Szilard engine. **(a)** A thin wall is inserted without any work cost. **(b)** The particle is found on one side through measurement. **(c)** Work is done to an external load through isothermal expansion. **(d)** The system is reset to its original state. Adapted from Fig. 1 in Ref. [4].

entropy increase somewhere else, greater than or equal to $k_B \ln 2$. Szilard ascribed this entropy increase to the measurement process and claimed $k_B \ln 2$ of entropy production to be a fundamental lower limit for this process [1].

A point that can be raised regarding the cyclic process described in this section is whether thermodynamics is applicable when the working medium consists of only a single particle. To solve this problem, one may instead view the system as an ensemble of identical systems [2], where the behaviour of the ensemble corresponds to that of an average single-particle system.

2.1.3 Erasure

The next major event in the history of Maxwell's demon occured in 1961, when Rolf Landauer published a paper on the lower bound of heat and entropy generation in computers [13]. Here, Landauer defines the concept of logical irreversibility for computing processes, *i.e.* processes with non-injective mapping between states. That a process is non-injective means that different initial states may end up in the same

final state for the same process.

To emphasize clarity, I will in the following paragraphs write every logical STATE with a special font.

Consider as an example the operation of memory erasure, which takes an arbitrary state to some reference ZERO state. This process is obviously not logically reversible if there are two or more states, since, when the system is found in ZERO, it is impossible to know which state the system was in prior to erasure. On the other hand, a logical operator such as the NOT-operator is logically reversible since it is always possible to know the state of the system before the operation (TRUE if FALSE and vice versa).

According to Landauer, every logical state must have some physical realization, which means that any logically irreversible process must cause a reduction in real, physical degrees of freedom and thus dissipation of heat [13].

To see why erasure must come with dissipation, let us examine an example more closely. For the Szilard engine, let the memory of the demon be similar to that of the engine itself, *i.e.* a single particle in a container of volume V divided into two equal parts by a partition. After the memory has been coupled to the engine the particle is on either side of the partition, corresponding to two different memory states: LEFT or RIGHT. By choosing LEFT to be the standard reference state, a process that causes erasure can be performed by first removing the partition and then compressing the gas from the right in a quasi-static and isothermal fashion. Here, the erasure operation requires work $k_B T \ln 2$ to be provided which dissipates as heat to the reservoir, increasing the entropy of the reservoir by $k_B \ln 2$. When this process is complete, the particle is definitely on the left side of the partition and the memory has been reset to the LEFT state regardless of the state prior to erasure [14].

Now, why can we not use a better erasure protocol in this example? If the memory is in the LEFT state before erasure, nothing needs to be done, and so only measurements which cause the memory to end up in the RIGHT state need to be reset. The answer is that, in order to make use of such a selective protocol, further measurements would have to be made. The memories corresponding to these measurements would subsequently have to be reset and so forth, resulting in a protocol that does not improve the erasure operation in terms of work efficiency and entropy production [2].

Roughly two decades after the aformentioned article by Landauer was published, Charles Bennett showed that the entropy production for a two-state process—such as the single-particle Szilard engine—can be made arbitrarily small [15]. By connecting these results about measurement and erasure to the Szilard engine, we see that the process described in section 2.1.2 is not cyclic. For it to be truly cyclic, the memory that stores the information gained through measurement in the second step has to

be reset. This requires (at least) work $k_B T \ln 2$ to be invested, exactly the amount obtained from the expansion process. Additionally, the entropy of the heat reservoir is increased by an amount larger than or equal to $k_B \ln 2$ due to heat dissipation. This entropy compensates for the 'missing' entropy in the cycle of the Szilard engine. Using Bennett's results on measurements, we see that it is the erasure process—not measurement as thought by Szilard—that saves the second law [14].

2.2 The Classical Many-Particle Szilard Engine

So far, only an engine with a single particle has been considered. In this section I will examine the classical Szilard engine (CSZE) with an arbitrary amount of particles assumed to obey the ideal gas law.

I will study a CSZE of volume V with a constant cross section A and a working medium consisting of N particles. The total length of the engine is L_{tot} so that $V = AL_{\text{tot}}$. The insertion position of the partition that separates the volume into two is denoted x^{ins} and measured from one side along the length of the volume, so that the end points of the volume correspond to 0 and L_{tot}, see Fig. 2.2.

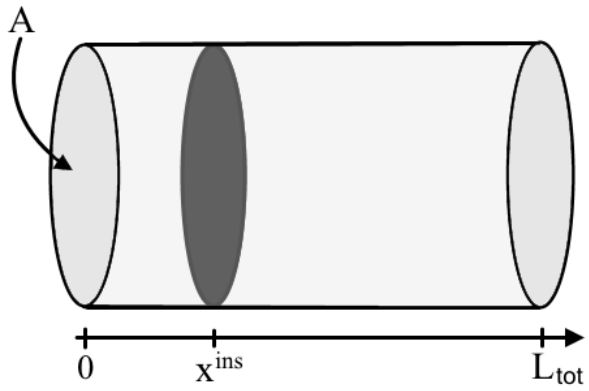

Figure 2.2: The volume of the Szilard engine described in the text, here a cylinder.

After insertion, the system is expanded to some position x_m^{rem}—based on the outcome of the measurement—and the partition is subsequently removed. Here m is the amount of particles found to the left of the partition after measurement. I will

in this section let the removal positions be at force balance, which from the ideal gas law can be obtained as $\{x_m/L_{\text{tot}}\} = \{m/N\}$.

Since the gas is assumed to be ideal, the particles are independent of each other and it is equally probable for a particle to occupy each point in the volume. The probability to find a particle in some partial volume $\tilde{V}$ of the system is then simply $\tilde{V}/V$. If the partition is inserted somewhere such that $0 < x^{\text{ins}} < L_{\text{tot}}$, the probability to find m particles to the left of it is

$$p_m(x^{\text{ins}}) = \binom{N}{m} \left(\frac{x^{\text{ins}}}{L_{\text{tot}}}\right)^m \left(1 - \frac{x^{\text{ins}}}{L_{\text{tot}}}\right)^{N-m}. \tag{2.2}$$

Here the factor $\binom{N}{m} = N!/(m!(N-m)!)$ is due to the particles being distinguishable.

When $m \neq 0$ and $m \neq N$ there are particles on both sides of the partition and thus pressure exerted from both sides. The work associated with the expansion when m particles are to the left of the partition is then

$$W^m_{\text{exp}}(x^{\text{ins}}) = \int_{Ax^{\text{ins}}}^{Vm/N} P^{(L)} dV' + \int_{V-Ax^{\text{ins}}}^{V-Vm/N} P^{(R)} dV', \tag{2.3}$$

where $P^{(L)}$ and $P^{(R)}$ are the pressures exerted from the particles in the left and right chambers, respectively. Since there are m particles to the left and $N-m$ particles to the right of the partition, we can by using the ideal gas write (2.3) as

$$W^m_{\text{exp}}(x^{\text{ins}}) = mk_BT \int_{Ax^{\text{ins}}}^{Vm/N} \frac{dV'}{V'} + (N-m)k_BT \int_{V-Ax^{\text{ins}}}^{V-Vm/N} \frac{dV'}{V'}, \tag{2.4}$$

which can be simplified to

$$W^m_{\text{exp}}(x^{\text{ins}}) = -k_BT \ln \left[\frac{\left(\frac{x^{\text{ins}}}{L_{\text{tot}}}\right)^m \left(1 - \frac{x^{\text{ins}}}{L_{\text{tot}}}\right)^{N-m}}{\left(\frac{m}{N}\right)^m \left(1 - \frac{m}{N}\right)^{N-m}} \right]. \tag{2.5}$$

When all particles are on either side of the partition the expansion work is simply

$$W^0_{\text{exp}}(x^{\text{ins}}) = Nk_BT \int_{V-Ax^{\text{ins}}}^{V} \frac{dV'}{V'} = -Nk_BT \ln \left(1 - \frac{x^{\text{ins}}}{L_{\text{tot}}}\right) \tag{2.6}$$

for $m = 0$ and

$$W^N_{\text{exp}}(x^{\text{ins}}) = Nk_BT \int_{Ax^{\text{ins}}}^{V} \frac{dV'}{V'} = -Nk_BT \ln \left(\frac{x^{\text{ins}}}{L_{\text{tot}}}\right) \tag{2.7}$$

for $m = N$.

If we assume the work associated with the insertion and removal processes to be zero as in the previous section, the total average work of a cycle is just the work of the expansions weighted with the probabilities (2.2), *i.e.*,

$$W_{\text{tot}} = \sum_{m=0}^{N} p_m(x^{\text{ins}}) W_{\text{exp}}^m(x^{\text{ins}}). \tag{2.8}$$

By combining (2.2), (2.5), (2.6) and (2.7) the total work is found to be

$$\begin{aligned} W_{\text{tot}} = &-Nk_BT\left[\left(\frac{x^{\text{ins}}}{L_{\text{tot}}}\right)^N \ln\left(\frac{x^{\text{ins}}}{L_{\text{tot}}}\right) + \left(1-\frac{x^{\text{ins}}}{L_{\text{tot}}}\right)^N \ln\left(1-\frac{x^{\text{ins}}}{L_{\text{tot}}}\right)\right] \\ &- k_BT \sum_{m=1}^{N-1} \binom{N}{m} \left(\frac{x^{\text{ins}}}{L_{\text{tot}}}\right)^m \left(1-\frac{x^{\text{ins}}}{L_{\text{tot}}}\right)^{N-m} \ln\left[\frac{\left(\frac{x^{\text{ins}}}{L_{\text{tot}}}\right)^m \left(1-\frac{x^{\text{ins}}}{L_{\text{tot}}}\right)^{N-m}}{\left(\frac{m}{N}\right)^m \left(1-\frac{m}{N}\right)^{N-m}}\right]. \end{aligned} \tag{2.9}$$

Since only the expansion process contributes to the total work of the CSZE, the removal positions at force balance must also be optimal with respect to maximizing the work output of the engine—expansion beyond force balance would go against the resulting force. To find the optimal work value with respect to the insertion position, the problem is studied numerically, see Fig. 2.3. Here it is found that the maximal work value is $k_BT \ln 2$, which is attained for $N = 1$ and $N = 2$, both at $x^{\text{ins}} = L_{\text{tot}}/2$. It may be concluded that the classical Szilard engine with non-interacting particles as a working medium can not exceed the amount $k_BT \ln 2$ in terms of work output.

2.3 The Quantum Szilard Engine

2.3.1 Introduction

One of the earliest treatments of a quantum Szilard engine (QSZE) was made by Zurek in 1984 [3], who studied a single particle in an infinite well in the high temperature limit (*i.e.* at temperatures high compared to the ground state energy). Zurek then continues on to reach conclusions similar to those made in the classical case.

A more recent study was made by Kim *et al.* [4], where they derive an expression for work output of the QSZE for arbitrary trapping potentials and temperatures. The results in this article are crucial for this thesis and I will in this section adapt

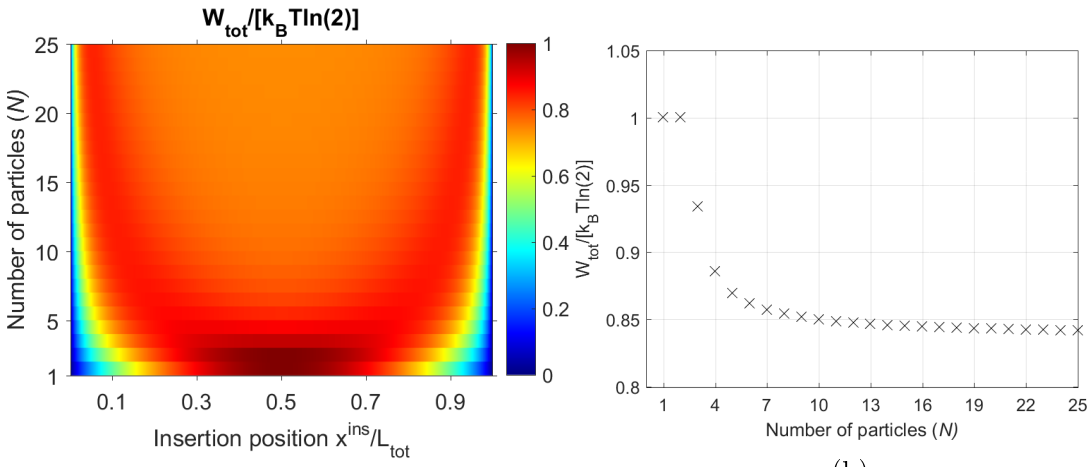

(a) (b)

Figure 2.3: Work output of the classical many-particle Szilard engine. **(a)** Work output relative to $k_B T \ln 2$ as a function of particle number and insertion position. **(b)** Optimal work output relative to $k_B T \ln 2$ as a function of particle number. From the left figure it can be seen that the CSZE is not very sensitive to the insertion position of the partition, and that this sensitivity is decreased with increasing particle number. In the right figure it can be seen that the optimal work output is a monotonically decreasing function in particle number.

a version of their derivation of the work output of the QSZE, *i.e.* closely following Ref. [4].

2.3.2 Work Output

In order to define the work performed by the QSZE, we assume a closed system with energy levels E_n according to the time-independent Schrödinger equation:

$$\hat{H} \left|\psi_n\right\rangle = E_n \left|\psi_n\right\rangle . \tag{2.10}$$

Here $\hat{H}$ is the Hamiltonian—which contains all information about the system, *e.g.* number of particles, trapping potential, interactions *etc.*—and $|\psi_n\rangle$ its eigenstates. If we denote the mean occupancies of each energy level by P_n, the internal energy U can be written as

$$U = \langle E \rangle = \sum_n P_n E_n, \tag{2.11}$$

which yields the differential

$$dU = \sum_n (P_n dE_n + E_n dP_n). \tag{2.12}$$

Next, we define (see Ref. [16])

$$\delta W \equiv -\sum_n P_n dE_n \quad \text{and} \quad \delta Q \equiv \sum_n E_n dP_n, \tag{2.13}$$

where δW and δQ are infinitesimal amounts of work and heat, respectively. The reasonability of these definitions can be argued for in the following way: We want the controllable part of the energy to be associated with work. If we change the Hamiltonian, we directly change the energy levels of the system. In doing so, the system can react by changing the occupancies of its states through excitations. This is done in an uncontrollable way and is thus associated with heat. The definitions (2.13) give us an expression that looks like the classical first law of thermodynamics, $dU = \delta Q - \delta W$, where work is defined positive if done *by* the system.

Assuming a quasi-static and isothermal process, the total amount of quantum thermodynamic work W performed as some external parameter (for example barrier height or position) is varied from X_1 to X_2 can be written as

$$W \equiv \int \delta W = -\sum_n \int_{X_1}^{X_2} P_n \frac{\partial E_n}{\partial X} dX. \tag{2.14}$$

Since the system is closed and the processes isothermal at some temperature T, the mean occupancies follow the Boltzmann distribution

$$P_n = \frac{e^{-\beta E_n}}{Z} = -\frac{1}{\beta}\frac{\partial \ln Z}{\partial E_n}, \tag{2.15}$$

where Z is the partition function $Z = \sum_n e^{-\beta E_n}$, and $\beta = 1/k_B T$. Using (2.15), (2.14) can be rewritten as

$$W = k_B T \sum_n \int_{X_1}^{X_2} \frac{\partial \ln Z}{\partial E_n}\frac{\partial E_n}{\partial X} dX = k_B T \int_{X_1}^{X_2} \frac{d \ln Z}{dX} dX. \tag{2.16}$$

If the partition function is continuous in the external parameter X, (2.16) may be further simplified to

$$W = k_B T[\ln Z(X_2) - \ln Z(X_1)]. \tag{2.17}$$

Identifying the Helmholtz free energy $F = -k_B T \ln Z$, we see that (2.17) can be written

$$W = F(X_1) - F(X_2) = -\Delta F. \tag{2.18}$$

This is the classical upper bound to the work performed according to the second law, $-\Delta F \geq W$, as expected for a quasi-static and isothermal process.

Armed with (2.17), we are now in a position to study the cycle of the QSZE. Just as in the classical case, the four steps of the cycle are insertion, measurement, expansion and removal (excluding erasure). The important difference here is that the insertion and removal processes change the energy levels of the system, which implies that there is a non-zero amount of work associated with these processes.

The insertion process is modelled by slowly increasing the height of an infinitely thin barrier. Just as in the previous section, the system is considered in a coordinate system on the interval $[0, L_{\text{tot}}]$, where L_{tot} is the total length of the box that the particles occupy. After insertion—but before measurement—the system is described by the partition function

$$Z(x^{\text{ins}}) = \sum_{m=0}^{N} Z_m(x^{\text{ins}}). \tag{2.19}$$

Here N is the total number of particles and $Z_m(x^{\text{ins}})$ the partition function of the system with m particles to the left of the barrier when the partition is inserted at the position x^{ins}, measured from zero in the coordinate system. The partition function describing the system before insertion is $Z_N(L_{\text{tot}}) = Z(L_{\text{tot}})$. Using (2.17) we find that the work associated with the insertion process is

$$W_{\text{ins}} = k_B T[\ln Z(x^{\text{ins}}) - \ln Z(L_{\text{tot}})]. \tag{2.20}$$

Following the insertion, a measurement is made—here assumed to cost no work—which puts the system in a state with a definite amount of particles on either side. The expansion is then performed by moving the partition quasi-statically to some position x_m^{rem}. Since the expansion is dependent on measurement outcome, there are up to $N+1$ different expansion positions x_m^{rem}, each one associated with the outcome where there are m particles to the left of the barrier. The average work of the expansion process then becomes

$$W_{\text{exp}} = k_B T \sum_{m=0}^{N} p_m(x^{\text{ins}})[\ln Z_m(x_m^{\text{rem}}) - \ln Z_m(x^{\text{ins}})]. \tag{2.21}$$

The prefactor $p_m(x^{\text{ins}}) \equiv Z_m(x^{\text{ins}})/Z(x^{\text{ins}})$ is the probability of finding m particles to the left of the partition as the measurement is performed.

During expansion, the barrier is assumed to be high enough so that tunnelling through the barrier can be neglected and the number of particles on each side remain constant and well-defined. Let this barrier height be denoted by V_∞. As the barrier is slowly removed, its height eventually reaches some value V_0, low enough to effect delocalization over both sides among the particles. At this point, the partition function describing the system is no longer $Z_m(x_m^{\text{rem}})$ but rather $Z(x_m^{\text{rem}})$. Since the partition function is no longer continuous in the barrier's height, (2.17) can not be used, and we have to instead take a step back and use (2.16). By separating the integral into two continuous parts, we can, for some specific measurement outcome, write

$$\frac{W_{\text{rem}}}{k_B T} = \int_{V_\infty}^{V_0} \frac{d \ln Z_m(x_m^{\text{rem}})}{dV} dV + \int_{V_0}^{0} \frac{d \ln Z(x_m^{\text{rem}})}{dV} dV \tag{2.22}$$

where V is the height of the barrier. Since the removal process is assumed to be quasi-static, $V_0, V_\infty \to \infty$ and the first term in (2.22) goes to zero. The average work associated with removal is therefore

$$W_{\text{rem}} = k_B T \sum_{m=0}^{N} p_m(x^{\text{ins}}) [\ln Z(L_{\text{tot}}) - \ln Z(x_m^{\text{rem}})]. \tag{2.23}$$

Summing up all the different parts of the work from the insertion, expansion and removal processes, we obtain the total work output of the QSZE as

$$W_{\text{tot}} = -k_B T \sum_{m=0}^{N} p_m(x^{\text{ins}}) \ln \left(\frac{p_m(x^{\text{ins}})}{p_m^*(x_m^{\text{rem}})} \right). \tag{2.24}$$

The function $p_m^*(x_m^{\text{rem}})$ has the same mathematical form as $p_m(x^{\text{ins}})$, *i.e.* $p_m^*(x_m^{\text{rem}}) \equiv Z_m(x_m^{\text{rem}})/Z(x_m^{\text{rem}})$. The asterisk here indicates the functions' different physical interpretations: The first one, $p_m(x^{\text{ins}})$, is the probability to find m particles to the left if the partition is inserted at the position x^{ins}, while $p_m^*(x_m^{\text{rem}})$ is the probability to find m particles to the left in a time-reversed process when the partition is inserted at x_m^{rem} [10]. A consequence of the possibility for the removal positions to be different is that the sum of the time-reversed probabilities $p_m^*(x_m^{\text{rem}})$ does not equal to one in general, *i.e.* $\sum_{m=0}^{N} p_m^*(x_m^{\text{rem}}) \neq 1$.

It should be noted that although the expression for work output (2.24) was derived for a quantum Szilard engine, it turns out to hold for a classical one as well [5]. While it is expected for quantum mechanics to contain classical mechanics, it is important

to remember that the irreversibility term containing p^* in (2.24) appeared as a result of quantum tunnelling. It turns out that there is a similar term in the classical case, but here this term is instead due to free expansion [5].

As a final side remark, I want to mention that there have been differing opinions about the removal process of the QSZE. In a comment by Plesch *et al.* [17], it is claimed that the work output of the QSZE should be higher than the amount obtained in [4], *i.e.* the work expression (2.24). This is further discussed in Ref. [8]. In a reply to these claims [18], Kim *et al.* remark that the results of Plesch *et al.* are due to them not accounting for the discontinuity of the partition function. This discontinuity leads to irreversibility and loss of work during the removal process [10].

Chapter 3

Theory and Method

As seen in the previous chapter, the only thing we need to know in order to obtain the total work output of the Szilard engine is the system's energies. When the energies are known, they can be used to construct the partition functions needed in order to obtain the probabilities in (2.24), which then give the total work.

I will in this chapter describe the method used to obtain the results in chapters 4 and 5, and give short reviews of the most pertinent theoretical concepts.

3.1 Identical Particles

The quantum-mechanical description of systems consisting of identical particles is treated in many different textbooks, and I will base this brief section on Refs. [19–21].

3.1.1 Basic Results

In the realm of quantum mechanics, two particles of the same kind are truly indistinguishable [19]. For some orthonormal basis $\{|\varphi_n\rangle\}$ of one-body states, the most general form of the many-body state describing a system of N particles can be written as

$$|\Psi\rangle = \sum_{n_1 \cdots n_N} c_{n_1 \cdots n_N} |\varphi_{n_1}\rangle \cdots |\varphi_{n_N}\rangle \,. \tag{3.1}$$

The permutation operator $\hat{P}_{ij}$ that interchanges the one-body state at position i in the tensor product with the one at position j is defined as

$$\begin{aligned}\hat{P}_{ij}\left|\Psi\right\rangle &= \hat{P}_{ij}\sum_{n_1\cdots n_N} c_{n_1\cdots n_N}\left|\varphi_{n_1}\right\rangle\cdots\left|\varphi_{n_i}\right\rangle\cdots\left|\varphi_{n_j}\right\rangle\cdots\left|\varphi_{n_N}\right\rangle \\ &= \sum_{n_1\cdots n_N} c_{n_1\cdots n_N}\left|\varphi_{n_1}\right\rangle\cdots\left|\varphi_{n_j}\right\rangle\cdots\left|\varphi_{n_i}\right\rangle\cdots\left|\varphi_{n_N}\right\rangle . \end{aligned} \tag{3.2}$$

We can immediately see that the permutation operator satisfies $\hat{P}_{ij}^2 = \mathbb{1}$, *i.e.* $\hat{P}_{ij} = \hat{P}_{ij}^{-1}$, where $\mathbb{1}$ is the identity operator. It turns out that the eigenvalues of the permutation operator are always $+1$ or -1, and that the eigenvalues of $\hat{P}_{ij}$ are the same for every i, j for some physical state [20]. Thus, it makes sense to define that

$$\begin{aligned}\left|\Psi\right\rangle \text{ is symmetric if } \hat{P}_{ij}\left|\Psi\right\rangle &= +\left|\Psi\right\rangle , \\ \left|\Psi\right\rangle \text{ is anti-symmetric if } \hat{P}_{ij}\left|\Psi\right\rangle &= -\left|\Psi\right\rangle ,\end{aligned}$$

where this type of symmetry is known as exchange symmetry. Since the expectation value of some observable $\hat{A}$ is independent of permutations (otherwise there would be some measurable quantity due to permutations, and the particles would not be indistinguishable) we must have

$$\left\langle\Psi\right|\hat{P}_{ij}^{\dagger}\hat{A}\,\hat{P}_{ij}\left|\Psi\right\rangle = \left\langle\Psi\right|\hat{A}\left|\Psi\right\rangle . \tag{3.3}$$

This can be extended to two arbitrary states $\left|\Psi\right\rangle$ and $\left|\Phi\right\rangle$ by writing [20]

$$\begin{aligned}\left\langle\Psi\right|\hat{A}\left|\Phi\right\rangle = \frac{1}{4}\Big(&\left\langle\Psi+\Phi\right|\hat{A}\left|\Psi+\Phi\right\rangle - \left\langle\Psi-\Phi\right|\hat{A}\left|\Psi-\Phi\right\rangle \\ &- i\left\langle\Psi+i\Phi\right|\hat{A}\left|\Psi+i\Phi\right\rangle + i\left\langle\Psi-i\Phi\right|\hat{A}\left|\Psi-i\Phi\right\rangle\Big),\end{aligned} \tag{3.4}$$

using short-hand notation according to $\left|\Psi+i\Phi\right\rangle = \left|\Psi\right\rangle + i\left|\Phi\right\rangle$. The expression (3.4) implies that $\hat{A} = \hat{P}_{ij}^{\dagger}\hat{A}\,\hat{P}_{ij}$. When $\hat{A} = \mathbb{1}$, we find that

$$\hat{P}_{ij} = \hat{P}_{ij}^{-1} = \hat{P}_{ij}^{\dagger}, \tag{3.5}$$

but since the permutation operator must be the same for every observable, (3.5) must be a general property, and hence $[\hat{A}, \hat{P}_{ij}] = 0$. In particular, when the observable is equal to the Hamiltonian, $\hat{A} = \hat{H}$, we have that the permutation operator is a conserved quantity from the Heisenberg equation of motion, which implies that exchange symmetry must be time-independent.

To the best of our knowledge, almost all systems of identical particles have a Hilbert space consisting of either only symmetric or only anti-symmetric states, which is known as the symmetry postulate [19] (there is a special type of quasiparticle called the anyon which is neither a boson nor a fermion [19]). Particles associated with symmetric states are known as bosons and particles associated with anti-symmetric states are known as fermions.

The fact that the many-body state is either symmetric or anti-symmetric imposes strong restrictions on its form. The bosonic many-body states $|\Phi^{(S)}\rangle$ are usually referred to as permanents, and must for N identical particles have the form [20]

$$|\Phi^{(S)}\rangle = \frac{1}{\sqrt{N!\prod_n N_n!}} \operatorname{perm} \begin{pmatrix} |\varphi_{n_1}\rangle^{(1)} & |\varphi_{n_2}\rangle^{(1)} & \cdots & |\varphi_{n_N}\rangle^{(1)} \\ |\varphi_{n_1}\rangle^{(2)} & |\varphi_{n_2}\rangle^{(2)} & \cdots & |\varphi_{n_N}\rangle^{(2)} \\ \vdots & \vdots & \ddots & \vdots \\ |\varphi_{n_1}\rangle^{(N)} & |\varphi_{n_2}\rangle^{(N)} & \cdots & |\varphi_{n_N}\rangle^{(N)} \end{pmatrix} \tag{3.6}$$

in order to be properly symmetrized. Here the upper index describes which space the ket belongs to, *i.e.* its position in the tensor product. The permanent (the mathematical object here denoted by 'perm', not the state $|\Phi^{(S)}\rangle$) is similar to the determinant except that it has plus signs where there are minus signs in the determinant. The numbers N_n denote how often a specific $|\varphi_n\rangle$ occurs in the tensor product. For example, if there are two particles in total, both in the same state $|\varphi_1\rangle$, then $N_1 = 2$ and $|\Phi^{(S)}\rangle = 1/2\,|\varphi_1\rangle\,|\varphi_1\rangle + 1/2\,|\varphi_1\rangle\,|\varphi_1\rangle = |\varphi_1\rangle\,|\varphi_1\rangle$ as expected.

The properly symmetrized fermionic many-body states $|\Phi^{(A)}\rangle$ are known as Slater determinants, and have for N identical particles the form [20]

$$|\Phi^{(A)}\rangle = \frac{1}{\sqrt{N!}} \begin{vmatrix} |\varphi_{n_1}\rangle^{(1)} & |\varphi_{n_2}\rangle^{(1)} & \cdots & |\varphi_{n_N}\rangle^{(1)} \\ |\varphi_{n_1}\rangle^{(2)} & |\varphi_{n_2}\rangle^{(2)} & \cdots & |\varphi_{n_N}\rangle^{(2)} \\ \vdots & \vdots & \ddots & \vdots \\ |\varphi_{n_1}\rangle^{(N)} & |\varphi_{n_2}\rangle^{(N)} & \cdots & |\varphi_{n_N}\rangle^{(N)} \end{vmatrix}. \tag{3.7}$$

As the states (3.6) and (3.7) are built out of single-particle states they do not include interactions between particles, and can therefore only describe the non-interacting case exactly. They can, however, be used as many-body basis states for systems with interactions, which will be described further in section 3.2.

3.1.2 Second Quantization

Although most of this section follows Ref. [21], the theory of second quantization can be found in most standard textbooks on many-particle quantum physics, see also for example Refs. [19, 20].

There is an alternative way to represent the many-body state, known as occupation number representation, which is used in the second quantization formalism. In second quantization, the many-body state is denoted by

$$|\Phi\rangle = |n_1, n_2, n_3, \ldots\rangle \tag{3.8}$$

where n_i is the number of particles with eigenvalue λ_i of some operator, for example the single particle Hamiltonian (λ_i is in this case the energy). As an example, let $\{|\varphi_n\rangle\}$ be a basis of single-particle states, then the many-body state for two particles where one particle is in $|\varphi_1\rangle$ and the other in $|\varphi_3\rangle$ can according to (3.6) and (3.7) be written as $1/\sqrt{2}(|\varphi_1\rangle\,|\varphi_3\rangle \pm |\varphi_3\rangle\,|\varphi_1\rangle)$, where the plus sign corresponds to bosons and the minus sign to fermions. Both of these states are in occupation number representation written simply as $|1, 0, 1, 0, 0, \ldots\rangle$, and the symmetry of the state is instead built into the operators in the formalism of second quantization, to be explained later in this section.

The states (3.8) belong to a space called the Fock space. A Fock space is a product of single-particle Hilbert spaces such that its elements are properly symmetrized [20].

One way to build the formalism of second quantization is to postulate that the states (3.8) satisfy both orthogonality and completeness and to introduce the operators $\hat{c}_i^\dagger$ and $\hat{c}_i$ such that these many-body states are eigenstates of the operator $\hat{c}_i^\dagger \hat{c}_i$ for all i. These operators are then postulated to follow the following (anti-)commutation relations [21]

Bosons	Fermions
$[\hat{c}_i^\dagger, \hat{c}_j^\dagger] = 0$	$\{\hat{c}_i^\dagger, \hat{c}_j^\dagger\} = 0$
$[\hat{c}_i, \hat{c}_j] = 0$	$\{\hat{c}_i, \hat{c}_j\} = 0$
$[\hat{c}_i, \hat{c}_j^\dagger] = \delta_{ij}$	$\{\hat{c}_i, \hat{c}_j^\dagger\} = \delta_{ij}.$

where the commutator and anti-commutator are defined as $[\hat{A}, \hat{B}] = \hat{A}\hat{B} - \hat{B}\hat{A}$ and $\{\hat{A}, \hat{B}\} = \hat{A}\hat{B} + \hat{B}\hat{A}$, respectively. From these relations it may be shown that the operators $\hat{c}_i^\dagger$ and $\hat{c}_i$ have the properties [20]

Bosons

$$\hat{c}_i^\dagger |n_1, n_2, \ldots, n_i, \ldots\rangle = \sqrt{n_i + 1}\, |n_1, n_2, \ldots, n_i + 1, \ldots\rangle$$
$$\hat{c}_i |n_1, n_2, \ldots, n_i, \ldots\rangle = \sqrt{n_i}\, |n_1, n_2, \ldots, n_i - 1, \ldots\rangle$$

and

Fermions

$$\hat{c}_i^\dagger |n_1, n_2, \ldots, 0_i, \ldots\rangle = (-1)^{\sum_{i<j} n_j} |n_1, n_2, \ldots, 1_i, \ldots\rangle$$
$$\hat{c}_i^\dagger |n_1, n_2, \ldots, 1_i, \ldots\rangle = 0$$
$$\hat{c}_i |n_1, n_2, \ldots, 0_i, \ldots\rangle = 0$$
$$\hat{c}_i |n_1, n_2, \ldots, 1_i, \ldots\rangle = (-1)^{\sum_{i<j} n_j} |n_1, n_2, \ldots, 0_i, \ldots\rangle .$$

It can be seen that the operator $\hat{c}_i^\dagger$ increases the amount of particles in state i, and that $\hat{c}_i$ decreases it. These operators are thus known as creation and annihilation operators. Together with the state (3.8), these operators contain the same information as the many-body states (3.6) and (3.7), but allow for a more tractable formalism, especially when a computational implementation is desired.

The position representation of a general one-dimensional many-body Hamiltonian without spin can be written

$$\hat{H} = \hat{H}^{(1)} + \hat{H}^{(2)} = \sum_{i=1}^{N} \left(-\frac{\hbar^2}{2M} \frac{d^2}{dx_i^2} + V^{(1)}(x_i) \right) + \frac{1}{2} \sum_{i \neq j} V^{(2)}(x_i, x_j) \tag{3.9}$$

where $\hbar$ is Planck's reduced constant, M the mass of single particle, $V^{(1)}$ an external one-body potential and $V^{(2)}$ a two-body interaction potential. The one-body Hamiltonian $\hat{H}^{(1)}$ corresponds to the first sum in the above expression and the two-body Hamiltonian $\hat{H}^{(2)}$ to the second sum. By using second quantization, this Hamiltonian may be rewritten as [21]

$$\hat{H} = \sum_{ij} \langle i| \hat{H}^{(1)} |j\rangle \hat{c}_i^\dagger \hat{c}_j + \sum_{ijkl} \langle ij| \hat{H}^{(2)} |kl\rangle \hat{c}_i^\dagger \hat{c}_j^\dagger \hat{c}_l \hat{c}_k \tag{3.10}$$

where

$$\langle i|\,\hat{H}^{(1)}\,|j\rangle = \int \phi_i^*(x)\hat{H}^{(1)}(x)\phi_j(x)dx \tag{3.11}$$

and

$$\langle ij|\,\hat{H}^{(2)}\,|kl\rangle = \int \phi_i^*(x)\phi_j^*(x')\hat{H}^{(2)}(x,x')\phi_k(x)\phi_l(x')dxdx', \tag{3.12}$$

where ϕ_i are the single-particle orbitals of the system. It is important to note that the transformation to the Hamiltonian written in terms of creation and annihilation operators (3.10) is valid only when the single-particle wave functions ϕ_i are orthogonal [20].

3.2 The Configuration Interaction Method

There are different numerical methods to obtain the energies of many-particle systems with interactions and I have for this thesis used the configuration interaction method (abbreviated CI). The reason for choosing this method is because it can be used to calculate the energies of excited states, unlike for example the Hartree-Fock method.

We want to obtain solutions to the time-independent Schrödinger equation (2.10), with a Hamiltonian of the form (3.9) as described in the previous section. Note that even though I restrict myself to one dimension in this section, both second quantization and CI can be used to treat system with more dimensions.

The first step of CI is to choose a suitable one-body basis $\{|\varphi_n\rangle\}$, for example the solutions to the one-body Schrödinger equation

$$\left(\frac{\hat{p}^2}{2M} + \hat{V}^{(1)}\right)|\varphi_n\rangle = \varepsilon_n\,|\varphi_n\rangle\,, \tag{3.13}$$

where $\hat{p}$ is the one-dimensional momentum operator and ε_n the single-particle energies. Using the one-body basis, a many-body basis $\{|\Phi_\nu\rangle\}$ can be constructed by forming the properly symmetrized many-body states. In order to be able to perform any calculations, the many-body basis has to be finite. This is not the case for many systems of interest, since the one-body bases of these systems are infinite, which implies that the many-body bases are also infinite. In order to proceed, a truncation has to be made. This truncation can, for instance, be made to either the one-body basis, many-body basis or both, by choosing only elements under a certain energy cut-off. Either way, the amount of elements in the many-body basis becomes finite. Let this size be denoted by d. By using this basis in conjunction with the completeness relation and Eq. (2.10), we obtain

$$\sum_{\nu=1}^{d} \langle \Phi_\xi | \hat{H} | \Phi_\nu \rangle \langle \Phi_\nu | \Psi^{(d)} \rangle = E^{(d)} \langle \Phi_\xi | \Psi^{(d)} \rangle \tag{3.14}$$

where $|\Psi^{(d)}\rangle$ and $E^{(d)}$ are the numerical approximations of $|\Psi\rangle$ and E due to the basis truncation. Equation (3.14) can be written in matrix form according to

$$\begin{pmatrix} \langle \Phi_1 | \hat{H} | \Phi_1 \rangle & \langle \Phi_1 | \hat{H} | \Phi_2 \rangle & \cdots & \langle \Phi_1 | \hat{H} | \Phi_d \rangle \\ \langle \Phi_2 | \hat{H} | \Phi_1 \rangle & \langle \Phi_2 | \hat{H} | \Phi_2 \rangle & \cdots & \langle \Phi_2 | \hat{H} | \Phi_d \rangle \\ \vdots & \vdots & \ddots & \vdots \\ \langle \Phi_d | \hat{H} | \Phi_1 \rangle & \langle \Phi_d | \hat{H} | \Phi_2 \rangle & \cdots & \langle \Phi_d | \hat{H} | \Phi_d \rangle \end{pmatrix} \begin{pmatrix} \langle \Phi_1 | \Psi^{(d)} \rangle \\ \langle \Phi_2 | \Psi^{(d)} \rangle \\ \vdots \\ \langle \Phi_d | \Psi^{(d)} \rangle \end{pmatrix} = E^{(d)} \begin{pmatrix} \langle \Phi_1 | \Psi^{(d)} \rangle \\ \langle \Phi_2 | \Psi^{(d)} \rangle \\ \vdots \\ \langle \Phi_d | \Psi^{(d)} \rangle \end{pmatrix}. \tag{3.15}$$

The problem is thus to find the matrix elements $\langle \Phi_\xi | \hat{H} | \Phi_\nu \rangle$ and to diagonalize the matrix in Eq. (3.15). By using the second quantization formalism, finding the matrix elements is reduced to finding which $\langle \Phi_\xi | \hat{H} | \Phi_\nu \rangle$ are non-zero and then calculating the one- and two-body matrix elements (3.11) and (3.12). The diagonalization can be done using standard numerical routines from, for example, the LAPACK library [22].

Typical numerical diagonalization methods have a time complexity proportional to d^3 for $d \times d$ matrices [23]. This becomes computationally expensive quickly with increased particle number. Consider an example where the size of the one-body basis is n and there are N particles. Without truncation in the many-body basis there are $\binom{n}{N}$ and $\binom{N+n-1}{N}$ elements in the many-body basis for fermions and bosons, respectively. In actual calculations we usually have $n \gg N$, so the many-body basis size is very rapidly increasing in N. For example: If the size of the one-body basis is $n = 100$, then there are 100 many-body basis states for one fermion, 4950 for two and 161700 for three. We can also conclude that it is computationally more expensive to perform calculations for bosonic systems than for fermionic when using equally sized one-body bases and no cut in the many-body basis.

3.3 Parity

The parity operator $\hat{\pi}$ in quantum mechanics is an operator that switches the sign of the position coordinate. The eigenvalues of $\hat{\pi}$ can readily be shown to be ± 1, so that we for eigenstates $|\psi\rangle$ of the parity operator have

$$\hat{\pi} |\psi\rangle = \pm |\psi\rangle . \tag{3.16}$$

By applying $\langle x|$ to Eq. (3.16) we get

$$\psi(-x) = \pm\psi(x). \tag{3.17}$$

Wave functions that correspond to the plus (minus) sign in (3.17) are said to have even (odd) parity.

For single-particle Hamiltonians $\hat{h}$ with external potentials that satisfy $V^{(1)}(x) = V^{(1)}(-x)$—which is, for example, the case for the infinite well or the harmonic oscillator—we immediately get that $[\hat{h}, \hat{\pi}] = 0$. In this case the solutions to Eq. (3.13) are simultaneous eigenstates of the Hamiltonian and the parity operator, and this property can be used to reduce the numerical effort when diagonalizing the Hamiltonian matrix. By separating the solutions to Eq. (3.13) into two sets of even and odd parity eigenstates, we can also divide the states of the resulting many-body basis by parity. If the many-body state $|\Phi\rangle = |\psi^{\text{even}}\rangle\,|\psi^{\text{odd}}\rangle$ consists of one even parity single-particle state and one odd (here omitting the symmetry of the state; every term in the Slater-determinant or permanent behaves in the same way), then it must itself have odd parity since

$$\Phi(x_1, x_2) = \langle x_1, x_2|\Phi\rangle = \langle x_1|\psi^{\text{even}}\rangle\,\langle x_2|\psi^{\text{odd}}\rangle = \psi^{\text{even}}(x_1)\psi^{\text{odd}}(x_2) \tag{3.18}$$

and

$$\Phi(-x_1, -x_2) = \psi^{\text{even}}(-x_1)\psi^{\text{odd}}(-x_2) = -\psi^{\text{even}}(x_1)\psi^{\text{odd}}(x_2) = -\Phi(x_1, x_2). \tag{3.19}$$

Assume now that the full system uses d many-body states. When the many-body states have been separated by parity, the many-body Schrödinger equation, *i.e.* Eq. (3.15), can be solved twice for each subset of many-body states. Since each subset has roughly half the amount of elements as the full system, the time complexity of the problem is reduced to $(d/2)^3 = d^3/8$ per subsystem, *i.e.* $d^3/4$ in total for some typical diagonalization routine. Since the time complexity for diagonalization of a system not divided by parity is d^3, we can see that the numerical effort of the diagonalization problem has been reduced significantly.

3.4 Method

The method described in this section can be used to obtain results for a QSZE with non-interacting particles as a medium or particles with contact-interactions

(the details of this type of interaction will be discussed later in this section). The notation used in this section follows that of section 2.3.2.

The expression (2.24) for work output of the Szilard engine was derived in section 2.3.2. It is important to remember that the processes in this derivation are carried out isothermally and quasi-statically. In order to find the work output of the QSZE for some specific system, the probabilities $p_m(x^{\text{ins}})$ and $\{p^*_m(x^{\text{rem}}_m)\}$ have to be calculated. As mentioned, both these probabilities have the same mathematical form, *i.e.*

$$p_m(x) = p^*_m(x) = \frac{Z_m(x)}{Z(x)}. \tag{3.20}$$

The partition function $Z_m(x)$ describes a system with m particles to the left of a partition inserted at x and $Z(x) = \sum_m Z_m(x)$. For a QSZE such that the subsystems to the left and right of the partition do not interact—which is the case for no interactions and contact-interactions (since the range of the contact-interaction is infinitely short, at least in theory)—we have that

$$E_{ij} = \varepsilon^{(L)}_i + \varepsilon^{(R)}_j. \tag{3.21}$$

Here E_{ij} are the energies of the full system and $\varepsilon^{(L)}_i$ and $\varepsilon^{(R)}_j$ the energies of the subsystems to the left and right of the partition that divides the system, respectively. The property (3.21) in conjunction with the assumption that the system can be described by the canonical ensemble allows us to write

$$Z_m(x) = \sum_{ij} e^{-\beta E_{ij}} = \sum_i e^{-\beta\varepsilon^{(L)}_i} \sum_j e^{-\beta\varepsilon^{(R)}_j} = Z^{(L)}_m(x) Z^{(R)}_{N-m}(L_{\text{tot}} - x) \tag{3.22}$$

where L_{tot} is the total length of the system considered, and N the total number of particles. The partition function $Z^{(L)}$ ($Z^{(R)}$) describes the subsystem to the left (right) of the partition that separates the composite system.

We can see that all we need in order to calculate the total partition function are the energies $\varepsilon^{(L/R)}_i$. Here $\varepsilon^{(L)}_i$ is the ith energy level of a system with m particles in the region $[0, x]$ to the left of the partition, and $\varepsilon^{(R)}_i$ the ith energy level of a system with $N - m$ particles in the region $[x, L_{\text{tot}}]$ to the right of the partition.

To calculate the energies $\varepsilon^{(L/R)}_i$, an external trapping potential has to be chosen to model the engine. In this thesis, the QSZE is modelled as a system that is eventually divided in two by a partition that is assumed to be an infinitely high and thin delta-like potential. The separation of the initial system yields two new subsystems, both described by Hamiltonians of the form (3.9).

The simplest choice for a trapping potential, and the one I am going to use throughout this thesis, is the infinite well described by the one-body potential

$$V^{(1)}(x) = \begin{cases} 0 & 0 < x < L_{\text{tot}}, \\ \infty & \text{otherwise.} \end{cases} \tag{3.23}$$

The benefits of using this potential to model the Szilard engine are many. Since it is infinite it has only bound states. Having only bound states can be seen as a requirement for this description of the engine since we want all particles to always belong to the engine so that the processes performed make sense in the original context of the Szilard engine. Additionally, due to the the potential's rectangular shape, it has a clear boundary, which is a useful property since there is only a well-defined finite region where the processes of the engine can be performed (for example, it is only meaningful to insert the partition that divides the system between the edges of the well, whereas, for instance, for the harmonic oscillator this is not as clear). Another useful property is that when the infinite well is separated by the delta-like partition, it is described by two new infinite wells. This means that all pertinent systems are described by infinite wells which can be exploited computationally.

In order to obtain good results, entire spectra of energies are needed, which makes the configuration interaction method an excellent choice for this task. Since the systems follow the canonical distribution, the lowest energy levels have the largest impact on the partition function. The amount of energy levels that are needed to accurately describe the partition function depends on the temperature of the heat reservoir. At low temperatures, the inverse temperatures $\beta = 1/k_B T$ are large, which means that terms corresponding to high energies in the partition function vanish quickly. It is thus possible to describe the partition functions accurately with fewer energy levels at low temperatures than at high. At high temperatures and, thus small β, more energy levels are needed which makes the calculations more computationally expensive.

In chapter 4 the particles' interactions are modelled with a contact-interaction. The contact-interaction—also known as the delta-interaction—is a good way to model the interactions of cold atoms [24]. Phenomenologically, it has the form

$$V^{(2)}(x_i, x_j) = g\delta(x_i - x_j), \tag{3.24}$$

where g is the interaction strength. A positive g corresponds to a repulsive interaction and a negative g to an attractive interaction ($g = 0$ means there is no interaction).

To present my results in a simpler way I have worked in dimensionless units. By introducing

$$\xi = \frac{10x}{L_{\text{tot}}} \tag{3.25}$$

to the Hamiltonian (3.9) and using (3.24) as the two-body potential, we get

$$\hat{H} = \frac{100\hbar^2}{L_{\text{tot}}^2 M}\left[\sum_{i=1}^{N}\left(-\frac{1}{2}\frac{d^2}{d\xi_i^2} + V^{(1)}(\xi_i)\right) + \frac{gL_{\text{tot}}M}{10\hbar^2} \times \frac{1}{2}\sum_{i\neq j}\delta(\xi_i - \xi_j)\right], \tag{3.26}$$

where L_{tot} is the physical length of the system. The reason for introducing the particular dimensionless unit of length in (3.25) is to transform the system from $0 \leq x \leq L_{\text{tot}}$ to a dimensionless system on the interval $0 \leq \xi \leq 10$ (*i.e.* to a new system where the wave functions vanish at $\xi = 0$ and $\xi = 10$). The number 10 in (3.25) is chosen simply so that the obtained energies are smaller (than they would be if we would have chosen 1) in terms of the new dimensionless units. It is the expression within the brackets of the Hamiltonian (3.26) that has been used in my calculations. As a result, energies are obtained in units of $100\hbar^2/(L_{\text{tot}}^2 M)$ and interaction strengths in units of $10\hbar^2/(L_{\text{tot}}M)$.

3.5 B-splines

B-splines are piecewise polynomials that can be defined according to [25]

$$B_{i,1}(x) = \begin{cases} 1 & t_i \leq x < t_{i+1} \\ 0 & \text{otherwise} \end{cases} \tag{3.27}$$

$$B_{i,k}(x) = \frac{x - t_i}{t_{i+k-1} - t_i}B_{i,k-1}(x) + \frac{t_{i+k} - x}{t_{i+k} - t_{i+1}}B_{i+1,k-1}(x) \tag{3.28}$$

where $B_{i,k}$ is a B-spline of index i and order k. The points t_i are called knot points and must satisfy $t_{i+1} \geq t_i$. B-splines of order $k = 2, 3, 4$ can be seen Fig. 3.1.

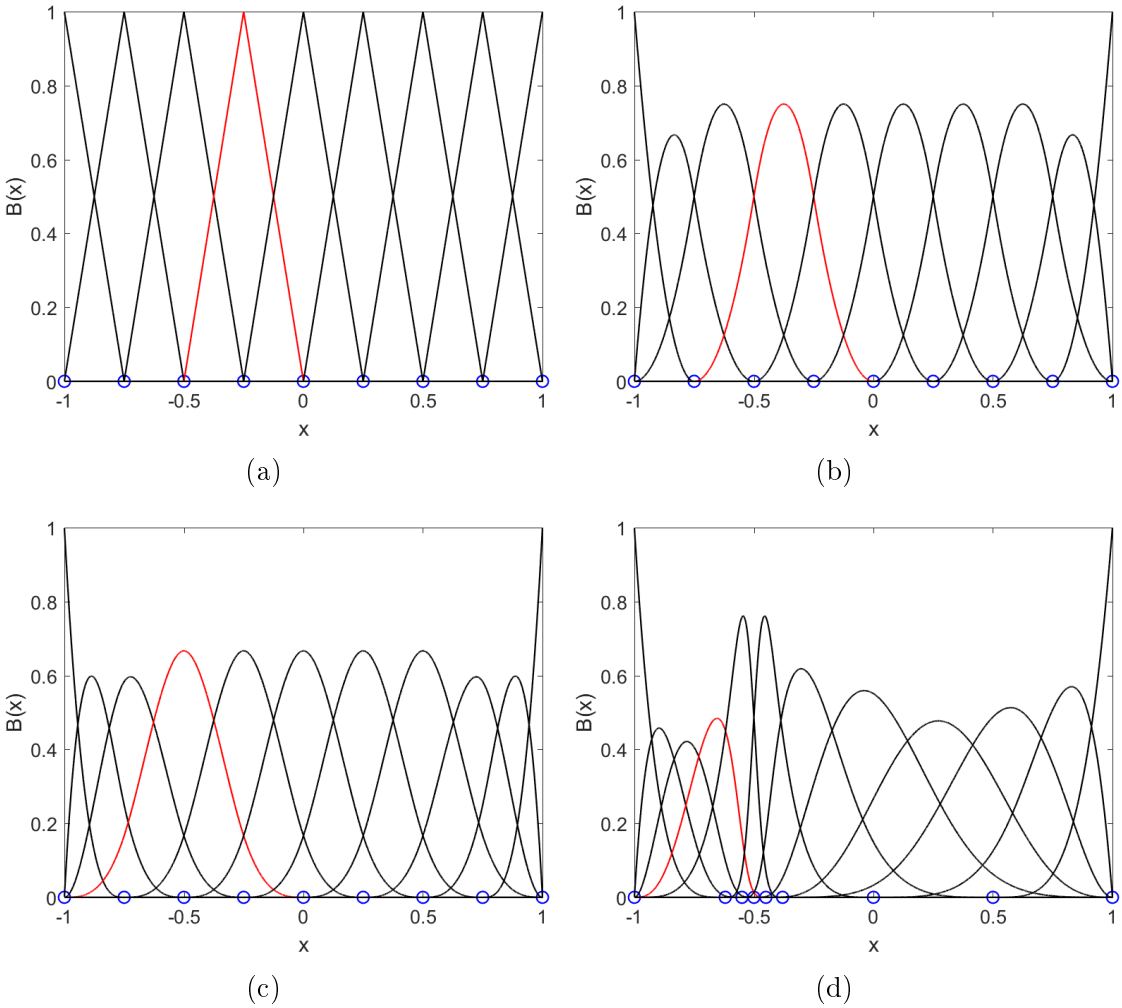

Figure 3.1: B-splines of different orders in the region $[-1, 1]$ with knot points marked by blue circles. Note that the boundary knot points are k times degenerate, where k is the order, so that the maximal amount of B-splines are defined everywhere. A single B-spline has been colored red to illustrate how it is non-zero only in some region. **(a)** B-splines of order two. **(b)** B-splines of order three. **(c)** B-splines of order four with a linear knot points distribution. **(d)** B-splines of order four where more knot points have been placed around $x = -0.5$.

Some properties of B-splines are that they are non-orthogonal and that $B_{i,k}(x)$ is non-zero only in the region $t_i < x < t_{i+k}$ [25], see Fig. 3.1. It follows from the definition that it is possible to have at most k B-splines that are non-zero at every

x, and in order to achieve this maximal value the boundary knot points have to be k times degenerate [25].

In the pre-existing CI code that I have used, B-splines are used as a basis. B-splines are not orthogonal, which is a requirement to be able to use the second quantization formalism that was introduced in section 3.1.2. In order to be able to use second quantization, the orthogonal one-body basis states $|\varphi_n\rangle$ are expressed as a linear combination of B-splines (it should be mentioned that we do not have to use the one-body basis, any orthogonal basis would do)

$$|\varphi_n\rangle = \sum_i c_{i,n} |B_i\rangle \,, \tag{3.29}$$

where $B_i(x) = \langle x|B_i\rangle$ (I will for simplicity omit the order index k from now on). Note that the expression (3.29) is an approximation since we are working with a finite amount of B-splines. The coefficients $c_{i,n}$ are then obtained by solving the Schrödinger equation in the B-spline basis. If $\hat{h}$ is the one-body Hamiltonian and ε_n its eigenvalues, we get, by projecting the Schrödinger equation onto the B-spline basis, the following equation:

$$\sum_i \langle B_j| \hat{h} |B_i\rangle \, c_{i,n} = \varepsilon_n \sum_i \langle B_j|B_i\rangle \, c_{i,n}. \tag{3.30}$$

This can be written in matrix form

$$\begin{pmatrix} \langle B_1| \hat{h} |B_1\rangle & \langle B_1| \hat{h} |B_2\rangle & \cdots \\ \langle B_2| \hat{h} |B_1\rangle & \langle B_2| \hat{h} |B_2\rangle & \cdots \\ \vdots & \vdots & \ddots \end{pmatrix} \begin{pmatrix} c_{1,n} \\ c_{2,n} \\ \vdots \end{pmatrix} = \varepsilon_n \begin{pmatrix} \langle B_1|B_1\rangle & \langle B_1|B_2\rangle & \cdots \\ \langle B_2|B_1\rangle & \langle B_2|B_2\rangle & \cdots \\ \vdots & \vdots & \ddots \end{pmatrix} \begin{pmatrix} c_{1,n} \\ c_{2,n} \\ \vdots \end{pmatrix}, \tag{3.31}$$

where

$$\langle B_j| \hat{h} |B_i\rangle = \int B_j(x) \hat{h} B_i(x) dx \tag{3.32}$$

and

$$\langle B_j|B_i\rangle = \int B_j(x) B_i(x) dx. \tag{3.33}$$

The integrals (3.32) and (3.33) are evaluated numerically using Gaussian quadrature, which is a numerical method of integration that can be used to obtain results to machine accuracy for polynomials [26].

In order to force the wave functions to vanish at the boundary, we remove the two B-splines that are non-zero at the boundary. Since the wave function is expanded in B-splines it is thus guaranteed to go to zero at the boundary.

Since B-splines are non-zero only in some region depending on its order, the Hamiltonian matrix becomes sparse and banded. Banded matrices do not require much memory to store and can be diagonalized efficiently using, for example, the LAPACK library [22] (which is what was used here).

Another benefit of using B-splines as basis is that the knot points can be placed to fit the system. If there are some regions that require more accuracy, more knot points can be placed there and vice versa, *i.e.* less points can be placed in regions that are not as interesting, see Figs. 3.1c and 3.1d for an example.

To obtain the results in this thesis I have in all cases used a linear knot point distribution inside the infinite well with B-splines of order $k = 5$. The many-body basis sizes used for my calculations varied depending on the type of system, see table 3.1.

	Bosons	Fermions
Two particles	5253	5151
Three particles	30856	27720

Table 3.1: Number of many-body basis states used in my calculations.

One may at this point ask why I have used B-splines as a basis over the analytically known infinite well solutions. The main reason is simply that there existed CI code available for me to use that utilizes the B-splines as a basis. A comparison of the accuracy between when B-splines and infinite well solutions are used as a basis can be seen in Fig. 3.2. The system used for this comparison consists of two bosons in an infinite well with an attractive contact-interaction. It can be seen that the infinite well solutions and the B-splines are very similar in terms of accuracy, but for my calculations the B-splines had significantly shorter runtimes.

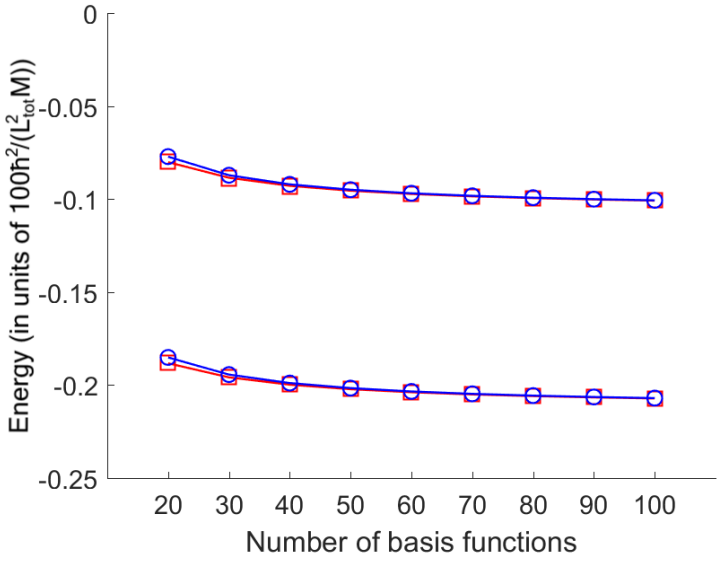

Figure 3.2: Comparison between B-splines and infinite well solutions as a basis. Shown are the two lowest energy levels of a system with two bosons in an infinite well with an attractive contact-interaction of interaction strength $g = -1.0 \times 10\hbar^2/(L_{\text{tot}}M)$. *Red squares:* Infinite well solutions. *Blue circles:* B-splines.

Chapter 4

Interactions

Many facets of the quantum Szilard engine have been studied in the literature, including general properties and work output [4], optimal conditions [10], the effect of spin [9], and the role of the third law of thermodynamics [6]. One aspect that has not yet been studied in great detail is how interactions affect the work output of the QSZE. The effect of some interactions is discussed briefly in Ref. [6], but a comprehensive study on the subject has yet to be made.

In this chapter I will study the QSZE for particles with contact-interactions and compare it to the non-interacting case.

4.1 No Interactions

Before we can examine how interactions affect the QSZE, results for the non-interacting case are needed as a reference, *i.e.* when $V^{(2)}(x_i, x_j) = 0$ in (3.9).

To obtain results for the QSZE with a non-interacting medium, it is not necessary to use the configuration interaction method since the single-particle energy levels of the infinite well are known analytically. The many-body energy levels are then just sums of different single-particle energy levels with degeneracies determined by particle type and spin.

The work output for two and three bosons and fermions as a function of temperature and insertion position can be seen in Fig. 4.1. Temperatures will throughout chapters 4 and 5 be given in units of E_1^{tb}/k_B, where E_1^{tb} is the ground state energy of the non-interacting two-boson system without any partition. This way, the temperatures are the same for all figures and the data can be compared directly. The particles are assumed to be spinless (although spinless fermions do not exist, they can be interpreted as a system of spin-polarized fermions). In these results, optimal

removal positions x_m^{rem} are used. It turns out that the optimal removal positions are not at force balance, which is an interesting peculiarity of quantum mechanics [10]. To obtain the removal positions that maximize work output in practice, I calculated the value of W_{tot} for many different removal positions over the whole interval $[0, L_{\mathrm{tot}}]$. How the optimal removal position for a QSZE with three particles varies with temperature can be seen in Fig. 4.2. Here the insertion position is chosen to be $x^{\mathrm{ins}} = L_{\mathrm{tot}}/2$ and the particle configuration such that there is one particle to the left of the partition. It can be seen from these results how the optimal removal position differs significantly from the classical limit $L_{\mathrm{tot}}/3$ at low temperatures but approaches it at high temperatures.

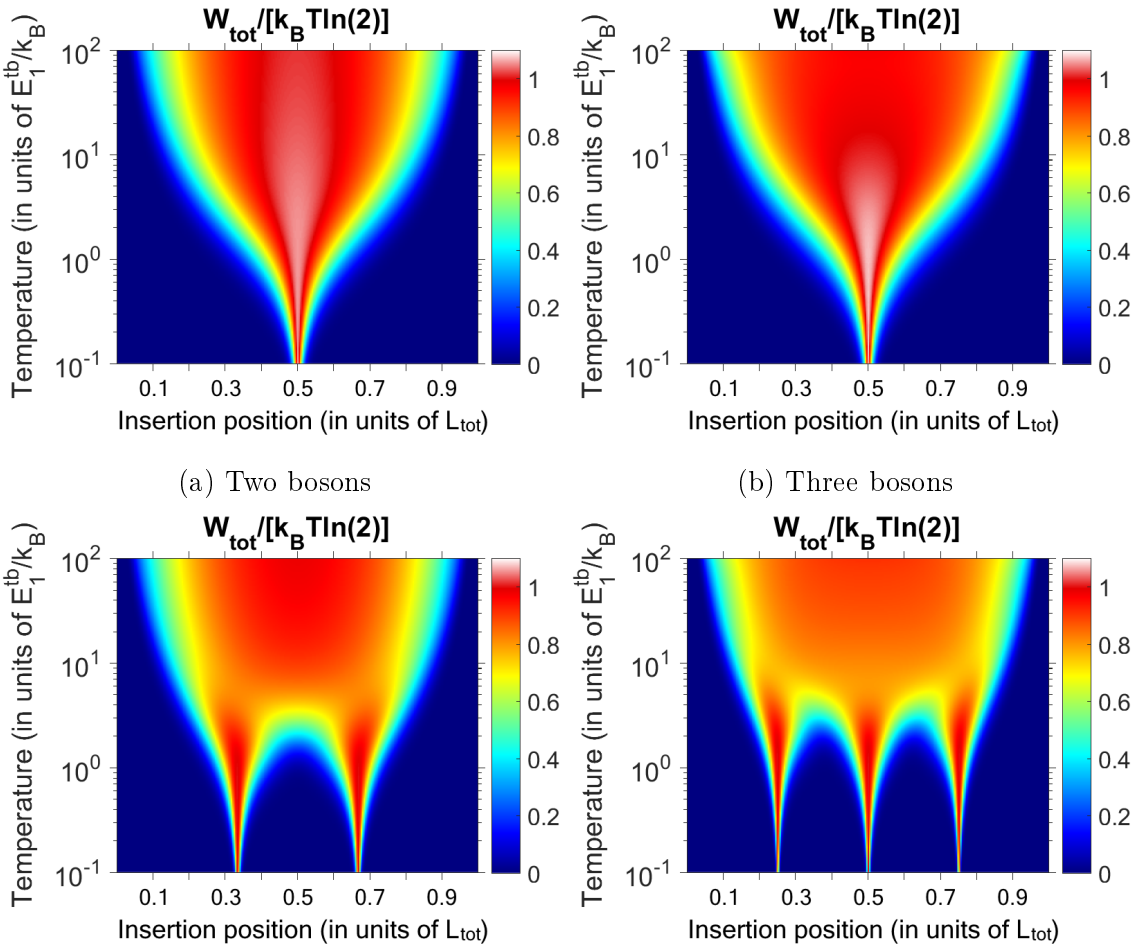

(a) Two bosons

(b) Three bosons

(c) Two fermions

(d) Three fermions

Figure 4.1: Work output of the QSZE with non-interacting particles as a function of barrier insertion position and temperature. At high temperatures it can be seen that the work output is similar for all systems. This can be explained by the QSZE approaching the classical limit at high temperatures, *i.e.* the results in Fig. 2.3a. At low temperatures W_{tot}/T is only non-zero at certain insertion points. For bosons it is only non-zero for a central insertion while for fermions it is non-zero at the same amount of points as the number of fermions.

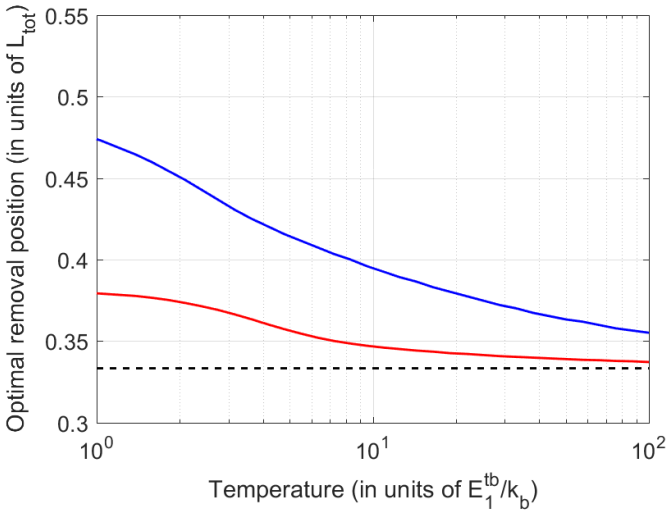

Figure 4.2: Optimal removal position as a function of temperature for three particles when there is one particle to the left of the partition and the partition is inserted at $x^{\text{ins}} = L_{\text{tot}}/2$. *Solid blue line:* Three bosons. *Solid red line:* Three fermions. *Dashed black line:* The classical optimal removal position $L_{\text{tot}}/3$.

In Fig. 4.1, the regions where the work output exceeds the classical upper bound $k_B T \ln 2$ are emphasized by white color. We see that it is possible for the quantum version of the Szilard engine to exceed the classical one in terms of work output, but only when the working medium consists of bosons. This is in agreement with the results in Ref. [4].

An interesting property of the QSZE is its low-temperature behaviour. As can be seen for all systems in Fig. 4.1, the work output divided by temperature, W_{tot}/T, approaches zero as the temperature approaches zero except at certain insertion positions. This can be understood in terms of the third law of thermodynamics, which claims that the entropy of a system approaches a constant value as the temperature approaches absolute zero. This value is non-zero if the ground state is degenerate and zero otherwise [27]. In Ref. [6], Kim and Kim show that the entropy production, which they define as

$$\Delta S = \sum_{m=0}^{N} p_m(x^{\text{ins}}) \ln \left(\frac{p_m(x^{\text{ins}})}{p_m^*(x_m^{\text{rem}})} \right), \tag{4.1}$$

vanish as $T \to 0$ unless the ground state of the system is degenerate. A perhaps more intuitive way to see it is to remember that the Szilard engine is driven by information.

The insertion position of the barrier may cause states such that the particles almost definitely are on one side of the barrier after insertion but before measurement, see Fig. 4.3. By combining this behaviour with the low temperature limit we get a system where it is known *a priori* which side of the partition the particles reside. There is thus no information to be extracted, and no fuel to drive the information heat engine. Consider as an example a two-boson QSZE directly after insertion with ground state energies $\varepsilon_1^{(L)}$ and $\varepsilon_1^{(R)}$ for the left and right subsystems respectively. In the $T \to 0$ limit the partition functions can be well approximated by the first term in the sum (if the energies of the subsystems are non-degenerate, which I will assume here) and the probability to find zero particles to the left of the partition after insertion becomes

$$p_0 = \frac{e^{-2\beta\varepsilon_1^{(L)}}}{e^{-2\beta\varepsilon_1^{(L)}} + e^{-\beta(\varepsilon_1^{(L)}+\varepsilon_1^{(R)})} + e^{-2\beta\varepsilon_1^{(R)}}} = \frac{1}{1 + e^{\beta(\varepsilon_1^{(L)}-\varepsilon_1^{(R)})} + e^{2\beta(\varepsilon_1^{(L)}-\varepsilon_1^{(R)})}}. \tag{4.2}$$

When the composite system is degenerate, *i.e.* when $\varepsilon_1^{(L)} = \varepsilon_1^{(R)}$, we get $p_0 = 1/3$, and in a similar way we find that $p_1 = p_2 = 1/3$. From (2.24) we get that the total work in this case reduces to

$$W_{\text{tot}} = \frac{k_B T}{3} \sum_{m=0}^{2} \ln(3p_m^*), \tag{4.3}$$

which can be larger than zero, depending on the time-reversed probabilities p_m^*. For the non-degenerate case, when the difference in ground state energies between the two subsystems satisfies $\varepsilon_1^{(R)} - \varepsilon_1^{(L)} \gg k_B T$, the exponentials in the denominator on the right-hand side in expression (4.2) vanish and we get $p_0 = 1$, and thus $p_1 = p_2 = 0$. The total work then becomes

$$W_{\text{tot}} = k_B T \ln(p_0^*) \leq 0, \tag{4.4}$$

which is only non-negative for $p_0^* = 1$.

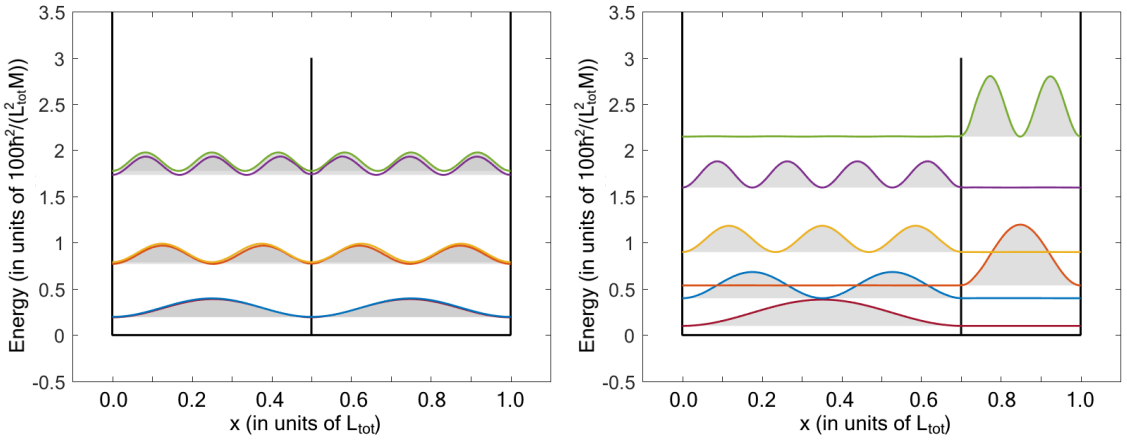

(a) (b)

Figure 4.3: Probability distributions of the six energetically lowest states for a single particle in an infinite well with a delta-type barrier of finite height. **(a)** Central barrier. Here the particle can be found on either side of the barrier with equal probability. **(b)** Displaced barrier. Here the particle is almost guarantueed to be found on one side of the barrier, depending on state.

The insertion positions that yield non-zero W_{tot}/T for the non-interacting QSZE can be predicted in terms of single-particle states. For bosons, all the particles in the engine occupy the lowest possible single-particle state in the $T \to 0$ limit. The only possibility to have a degenerate system is when the left and right wells are equal, so that the particles may be distributed in different ways between the wells while still having the same total energy. The only insertion position that yields non-zero W_{tot}/T is thus $x^{\text{ins}} = L_{\text{tot}}/2$—for any amount of non-interacting bosons.

For fermions, things get a little bit more complicated due to the exclusion principle. Consider the case of spin-polarized fermions. Again, all particles will in the zero-temperature limit occupy the lowest single particle states, up to the Fermi level. Thus for the system to be degenerate, the single-particle states have to be degenerate at the Fermi level. This degeneracy can be achieved when energy level i of the left well is the same as j of the right well, while simultaneously $i + j = N - 1$, where N is the total number of particles [7]. Together with the single-particle energy levels of the infinite well this gives a criterion for degeneracies according to

$$\frac{\hbar^2 i^2 \pi^2}{2ML_{\text{tot}}^2} = \frac{\hbar^2 j^2 \pi^2}{2M(L_{\text{tot}} - x^{\text{ins}})^2} \tag{4.5}$$

where x^{ins} is the insertion position. Using $i + j = N - 1$ we find that [7]

$$\frac{x^{\text{ins}}}{L_{\text{tot}}} = \frac{i}{N+1} \tag{4.6}$$

for $i = 1, \ldots, N$, which agrees well with the results in Fig. 4.1.

4.2 Contact-Interactions

In this section I will study the QSZE with contact-interacting bosons as a working medium to see if it is possible to improve the work output of the engine.

4.2.1 Insertion Position and Temperature Dependence for Bosons

When particles are on different sides of the partition they can never interact due to the infinitely short range of the contact-interaction, which means that the systems on either side of the partition can be treated separately. Results for some different values of the interaction strength g are shown in Figs. 4.4 and 4.5. Cross sections of some of these colormap-plots for two bosons can be seen in Fig. 4.6.

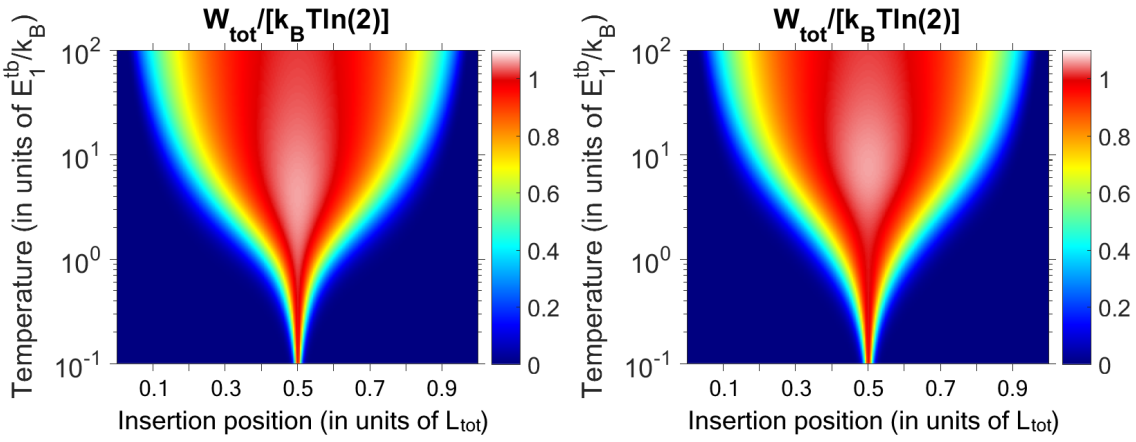

(a) $g = -0.5 \times 10\hbar^2/(L_{\text{tot}}M)$ (b) $g = -1.0 \times 10\hbar^2/(L_{\text{tot}}M)$

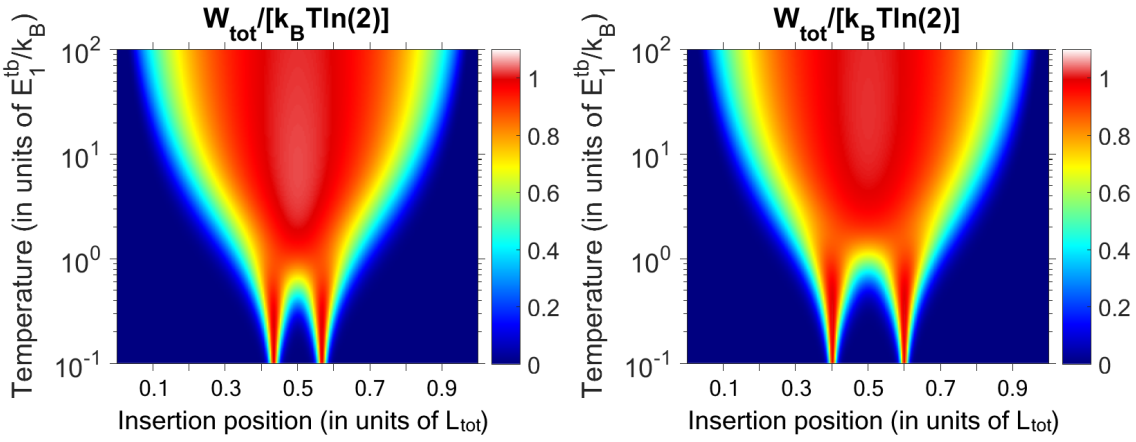

(c) $g = 0.5 \times 10\hbar^2/(L_{\text{tot}}M)$ (d) $g = 1.0 \times 10\hbar^2/(L_{\text{tot}}M)$

Figure 4.4: Work output as a function of temperature and barrier insertion position of the two-boson QSZE with a contact-interaction of different strengths. We can see that the work output has decreased for repulsive interactions in the regions that are white-colored in the non-interacting case. At low temperatures W_{tot}/T is only non-zero for a central insertion position for attractive interactions (*cf.* Fig. 4.1a). For repulsive interactions this is no longer the case and we instead see two non-zero points that are moved further away from each other with increased interaction strength, and the results begin to resemble the results in Fig. 4.1c.

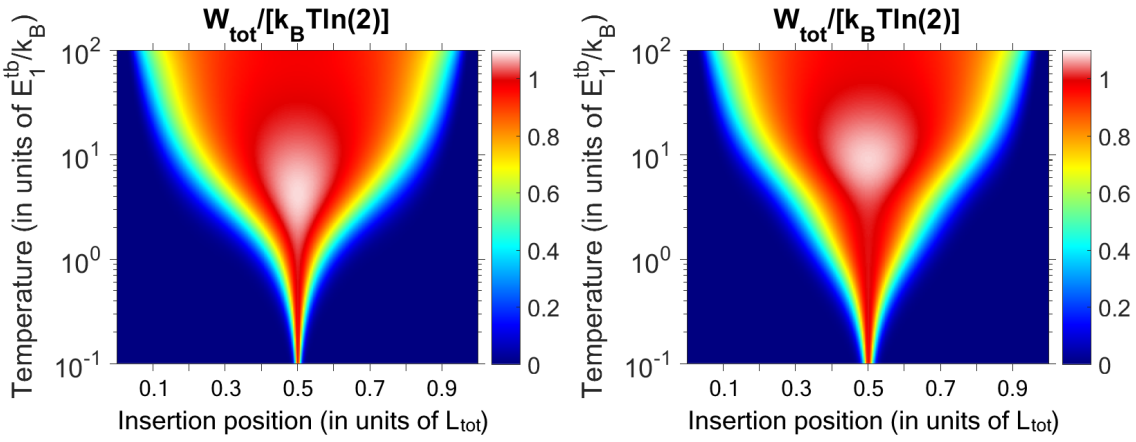

(a) $g = -0.5 \times 10\hbar^2/(L_{\text{tot}}M)$ (b) $g = -1.0 \times 10\hbar^2/(L_{\text{tot}}M)$

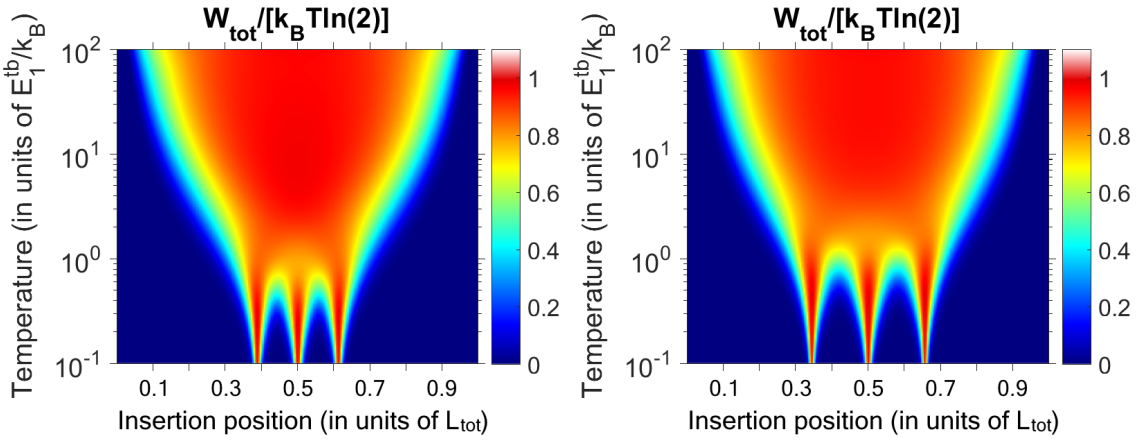

(c) $g = 0.5 \times 10\hbar^2/(L_{\text{tot}}M)$ (d) $g = 1.0 \times 10\hbar^2/(L_{\text{tot}}M)$

Figure 4.5: Work output as a function of temperature and barrier insertion position of the three-boson QSZE with a contact-interaction of different strengths. We can see that the work output has decreased for repulsive interactions in the regions that are white-colored in the non-interacting case. For attractive interactions this region is moved (*cf.* Fig. 4.1b). At low temperatures W_{tot}/T is only non-zero for a central insertion position for attractive interactions. For repulsive interactions we see that we now have three non-zero points that are moved further away from each other with increased interaction strength, and the results begin to resemble the results in Fig. 4.1d.

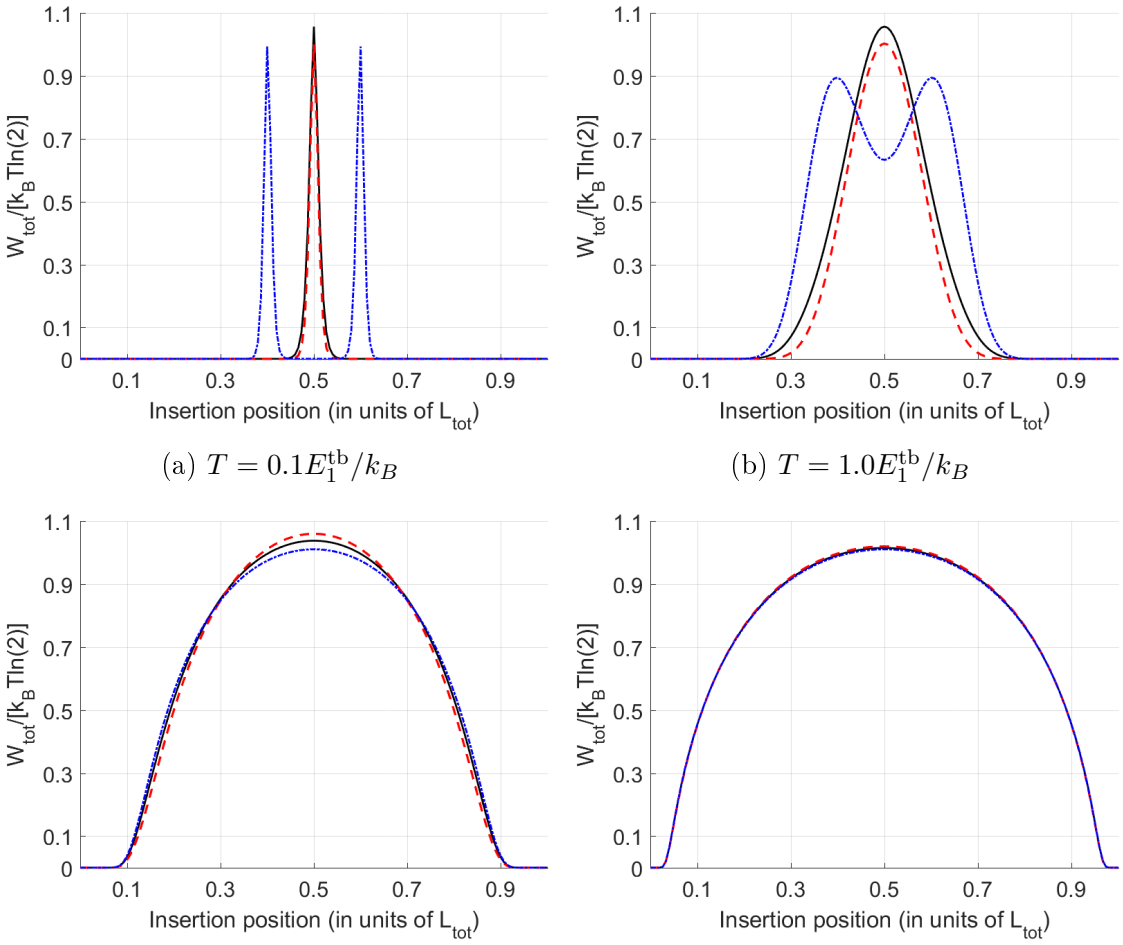

(a) $T = 0.1E_1^{\mathrm{tb}}/k_B$

(b) $T = 1.0E_1^{\mathrm{tb}}/k_B$

(c) $T = 10.0E_1^{\mathrm{tb}}/k_B$

(d) $T = 100.0E_1^{\mathrm{tb}}/k_B$

Figure 4.6: Work output of the two-boson QSZE as a function of barrier insertion position. *Black solid line:* $g = 0$. *Blue dashed-dotted line:* $g = 1.0 \times 10\hbar^2/(L_{\mathrm{tot}}M)$. *Red dashed line:* $g = -1.0 \times 10\hbar^2/(L_{\mathrm{tot}}M)$. The results show how the effects of interactions are most pronounced at low temperatures.

For repulsive interactions we see that as the interaction strength increases, the results look more and more like spinless fermions, *cf.* Figs. 4.1c and 4.1d. This is no coincidence, but rather a property of one-dimensional bosons with repulsive interactions. In the infinite repulsion limit, bosons act like spin polarized fermions. This limit is known as the Tonks-Giradeau regime [28]. A consequence of this behaviour is that the regions where the QSZE exceeds the classical maximum in terms of work output disappears.

For attractive interactions, it is hard to quantitatively determine the effects from these figures, and it is not clear if we can get any improvement in terms of work output due to interactions. The role of attractive interactions for bosons will thus be studied in some more detail in the next section.

4.2.2 Attractive Interaction Dependence for Bosons

A system that allows itself to be examined fairly easily is the two-boson QSZE. Because of the results of the previous section, where bosons act increasingly as fermions for repulsive interactions, I will in this section restrict myself to attractive interactions in order to see if it is possible to increase the work output via interactions.

For two bosons, the work output formula (2.24) can be simplified. When both particles are on either side, the optimal expansion protocol is to expand as far as possible, *i.e.* to the boundary of the full system. This implies that $p_0^* = p_2^* = 1$, and for symmetry reasons we also have $p_0 = p_2$. I am here interested in the optimal work output of the QSZE, and it may be shown that a central insertion position yields an extremum for work output as a function of insertion position [10]. That this is in fact a maximum for interaction strengths $g \leq 0$ is supported by the results that were presented previously in this chapter and can be confirmed numerically. By using $x^{\text{ins}} = L_{\text{tot}}/2$ we get $p_1 = p_1^*$, and the two-boson work output $W_{\text{tot}}^{\text{tb}}$ may be reduced to

$$W_{\text{tot}}^{\text{tb}} = -2k_B T p_0(g, x^{\text{ins}}(g)) \ln \left[p_0(g, x^{\text{ins}}(g)) \right] \tag{4.7}$$

where the probability p_0 is a function of interaction strength g and insertion position $x^{\text{ins}}(g)$. Note that in the general case, the insertion position may depend on the interaction strength. I will for this particular system assume that they do not, which can be confirmed numerically for optimal insertion positions. Taking the total derivative of (4.7) with respect to the interaction strength yields

$$\frac{dW_{\text{tot}}^{\text{tb}}}{dg} = -2k_B T \left(\frac{\partial p_0}{\partial g} + \frac{\partial p_0}{\partial x^{\text{ins}}} \cdot \frac{dx^{\text{ins}}}{dg} \right) (\ln p_0 + 1) \,, \tag{4.8}$$

but since x^{ins} was assumed to be independent of g, $dx^{\text{ins}}/dg = 0$ and

$$\frac{dW_{\text{tot}}^{\text{tb}}}{dg} = -2k_B T \frac{\partial p_0}{\partial g} (\ln p_0 + 1) . \tag{4.9}$$

From the definition of the probability $p_m = Z_m / \sum_n Z_n$ we find

$$\frac{\partial p_0}{\partial g} = \frac{Z_1}{(2Z_0 + Z_1)^2} \frac{\partial Z_0}{\partial g} < 0 \tag{4.10}$$

since the partition function describing the system when the particles are on different sides Z_1 is independent of interaction strength, $\partial Z_1/\partial g = 0$. As the energy levels increase for increased g, Z_0 must be strictly decreasing in g and the inequality above then follows from the positivity of the partition function.

The negativity of (4.10) implies that the derivative (4.9) is zero precisely when $p_0 = 1/e$. As shown by Kim *et al.* [4], $1/4 < p_0 < 1/3$ for two bosons without interactions. For interacting particles we have

$$p_0 = \frac{Z_0}{2Z_0 + Z_1} \to \frac{1}{2}, \quad g \to -\infty \tag{4.11}$$

if we assume that Z_0 increases with increased interactions strength to a point where $Z_0 \gg Z_1$. Since $1/3 < 1/e < 1/2$, the existence of extrema is guaranteed at any temperature, and (4.10) implies that there is only a single one. This is a maximum, since

$$\frac{d^2 W_{\text{tot}}^{\text{tb}}}{dg^2} = -2k_B T \left[\frac{\partial^2 p_0}{\partial g^2} (\ln p_0 + 1) \left(\frac{\partial p_0}{\partial g} \right)^2 \frac{1}{p_0} \right], \tag{4.12}$$

which at the point $p_0 = 1/e$ simplifies to

$$-2k_B T \left(\frac{\partial p_0}{\partial g} \right)^2 \frac{1}{p_0} < 0. \tag{4.13}$$

The optimal work output $W_{\text{opt}}^{\text{tb}}$ for the two-boson QSZE becomes

$$W_{\text{opt}}^{\text{tb}} = \frac{2}{e} k_B T. \tag{4.14}$$

The maximal work performed by the classical Szilard engine is $W_c = k_B T \ln 2$. It has been shown [4] that the maximal amount of work performed by the non-interacting two-boson QSZE is $W_{\text{ni}}^{\text{tb}} = (2/3) k_B T \ln 3$. This means that

$$W_{\text{opt}}^{\text{tb}} > W_{\text{ni}}^{\text{tb}} > W_c \tag{4.15}$$

with

$$W_{\text{opt}}^{\text{tb}} = \frac{2}{e \ln 2} W_c \approx 1.0615 W_c \quad \text{and} \quad W_{\text{opt}}^{\text{tb}} = \frac{3}{e \ln 3} W_{\text{ni}}^{\text{tb}} \approx 1.0046 W_{\text{ni}}^{\text{tb}}. \tag{4.16}$$

We can thus conclude that the two-boson Szilard engine has a unique maximal W_{tot}/T value with respect to attractive contact-interactions. At this maximum W_{tot}/T is the same regardless of temperature.

The work output as a function of interaction strength is shown in Figs. 4.7, 4.8 and 4.9. For two bosons, the theoretical results of this section are confirmed as the maximal W_{tot}/T value is found to be the same at any temperature. This maximal value is assumed for stronger interactions as the temperature increases.

For three bosons we can see that the behaviour of a common maximal value for W_{tot}/T is no longer present, but it is found that that the three-boson QSZE outperforms the CSZE also in the interacting case (since the QSZE transitions to the CSZE in the high-temperature limit). It may also be observed that the maximal work output for three bosons is larger than for two bosons. An interesting question is whether the work output of the interacting QSZE under optimal conditions increases with increased particle number. One might conjecture that this is the case since the engine is information driven and there are more possible outcomes for more particles. Unfortunately, due to computational limitations, I have not been able to study this any further for this master thesis.

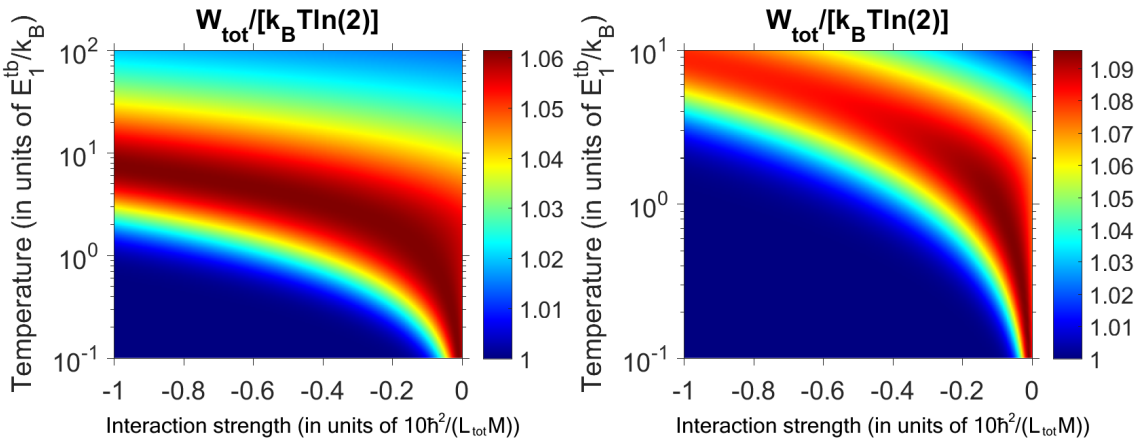

(a) Two bosons (b) Three bosons

Figure 4.7: Work output as a function of interaction strength and temperature. Note that the temperature scale is different for two and three bosons due to computational limitations in the three-boson case. For two bosons we can see that there is a constant maximal W_{tot}/T value that is independent of the interaction strength. This is not the case for three bosons, and this maximal value decreases with increasing temperature.

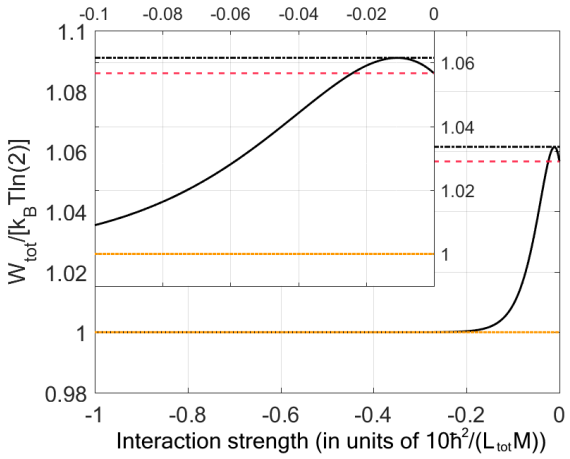

(a) $T = 0.1E_1^{\mathrm{tb}}/k_B$

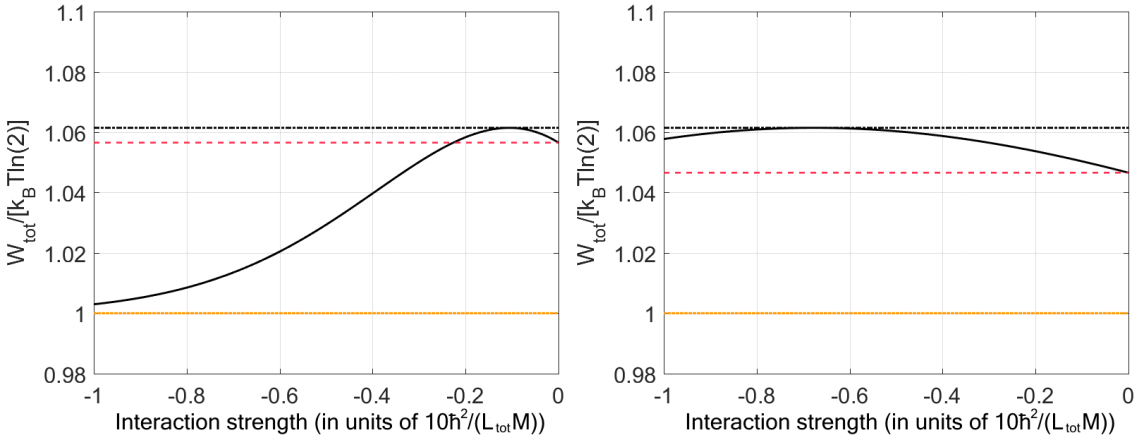

(b) $T = 1.0E_1^{\mathrm{tb}}/k_B$

(c) $T = 5.0E_1^{\mathrm{tb}}/k_B$

Figure 4.8: Work output as a function of interaction strength of the two-boson QSZE at some temperatures. The inset figure in **(a)** shows the same data over a smaller interval. *Yellow dotted line:* maximal work output of the CSZE $k_B T \ln 2$. *Red dashed line:* work output at zero interaction. *Black dashed-dotted line:* theoretical maximum for the two-boson QSZE with interacting particles $(2/e)k_B T$. The results show how the maximal W_{tot}/T value is achieved for stronger interaction strengths as the temperature increases.

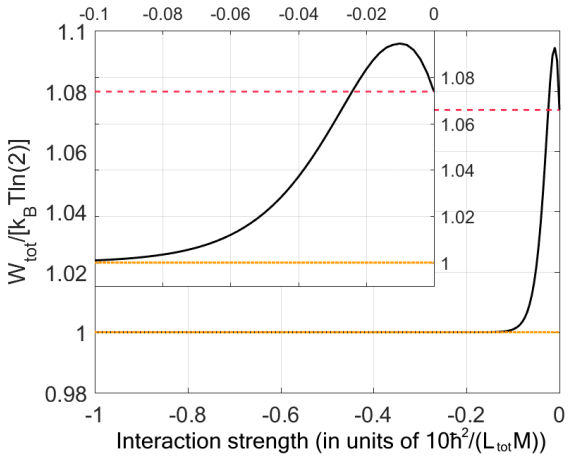

(a) $T = 0.1E_1^{\mathrm{tb}}/k_B$

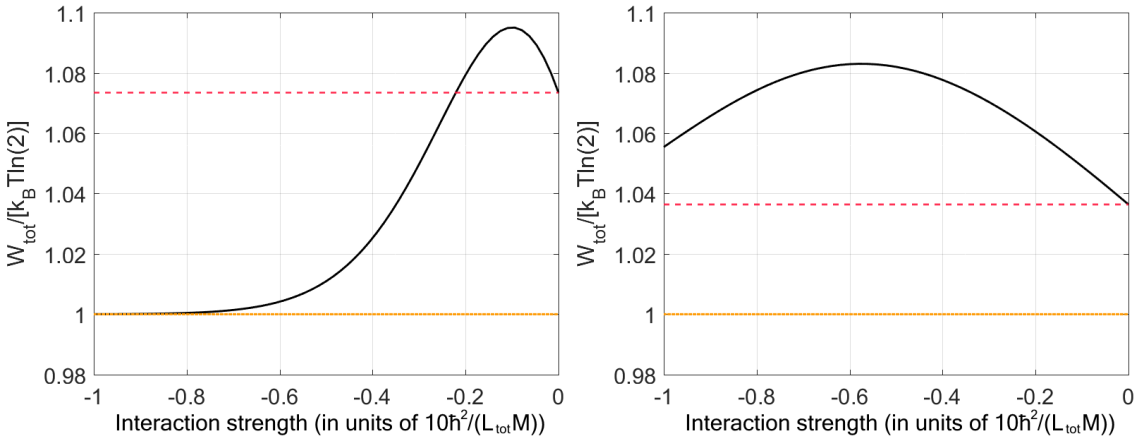

(b) $T = 1.0E_1^{\mathrm{tb}}/k_B$

(c) $T = 5.0E_1^{\mathrm{tb}}/k_B$

Figure 4.9: Work output as a function of interaction strength of the three-boson QSZE at some temperatures. The inset figure in **(a)** shows the same data over a smaller interval. *Yellow dotted line:* maximal work output of the CSZE $k_B T \ln 2$. *Red dashed line:* work output at zero interaction. The results show that the maximal W_{tot}/T value is lower for $T = 5.0E_1^{\mathrm{tb}}/k_B$ than for $T = 1.0E_1^{\mathrm{tb}}/k_B$ and $T = 0.1E_1^{\mathrm{tb}}/k_B$.

Chapter 5

Impurities

Something that may be interesting for the experimenter striving to realize a quantum version of the Szilard engine is the impact of anomalies in the equipment. By continuing on in the same fashion as the previous chapter, I will here study this phenomenon by adding a pertubation— here referred to as an impurity—to the confining potential of the QSZE.

The impurity will be modelled as a Gaussian function, *i.e.* by adding a potential of the form

$$V^{(1)}(x) = ae^{-(x-d)^2/(2\sigma^2)} \tag{5.1}$$

to the Hamiltonian describing the system (3.9). Here a, d and σ are constants that describe the amplitude, displacement and width of the Gaussian respectively. Removal positions will be chosen such that they maximize the work output of the engine.

The reason I have chosen a potential of the form (5.1) is simply because it is easy to implement numerically and can be customized intuitively through the parameters a, d and σ. Real impurities in experiments can vary in form and are not necessarily modelled well by (5.1).

Results for the two-boson QSZE with an added potential (5.1) with varying displacement d are shown in Fig. 5.1. Results for the same system with different amplitudes a can are shown in Fig. 5.2.

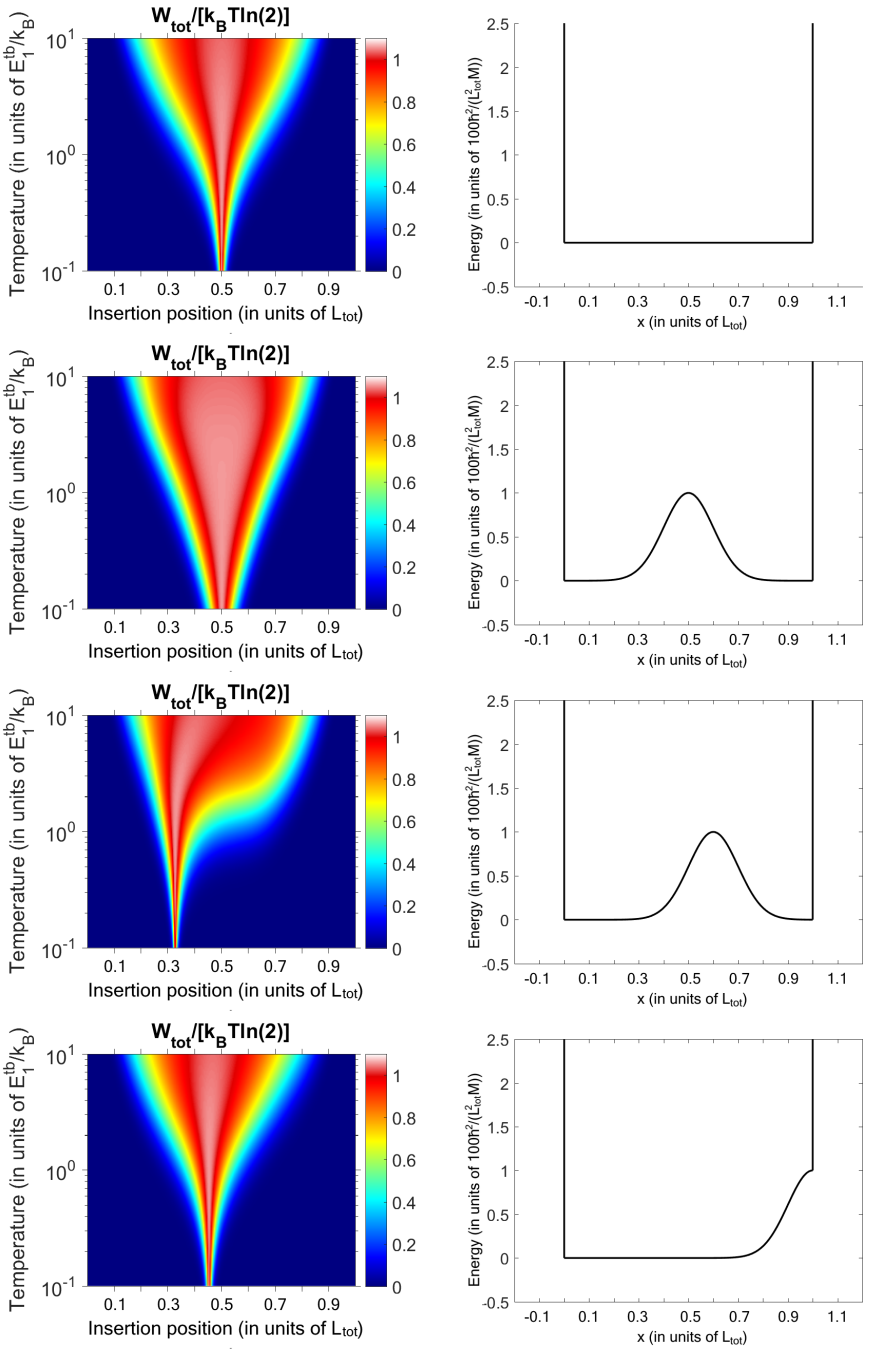

Figure 5.1: Work output as function of temperature and insertion position of the two-bosons QSZE with and without an impurity. The impurity is described by a Gaussian according to the well in the right column. The results show how W_{tot}/T is strongly dependent on the impurity's position at low temperatures.

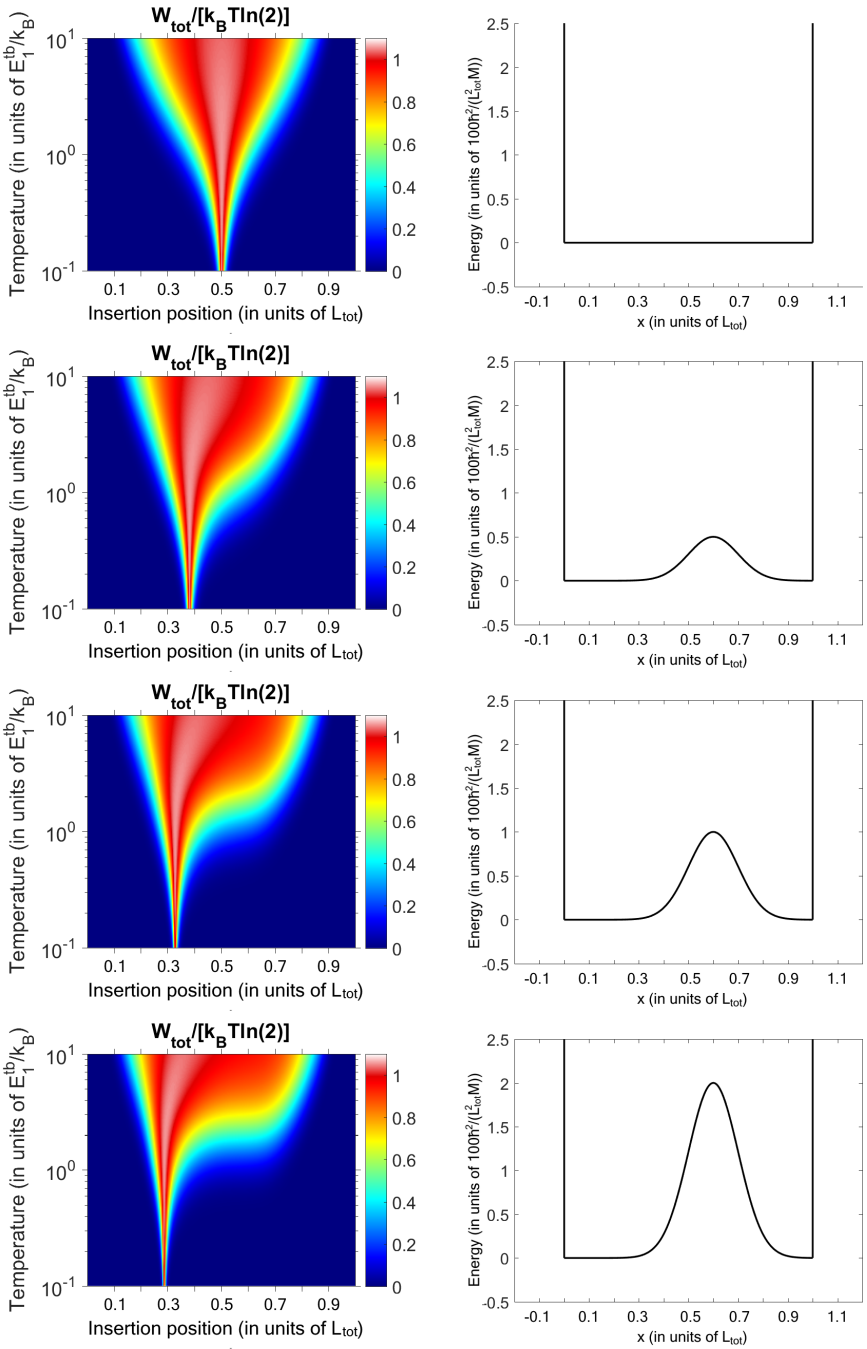

Figure 5.2: Work output as function of temperature and insertion position of the two-bosons QSZE with and without an impurity. The impurity is described by a Gaussian according to the well in the right column. It can be observed that as the impurity grows in size, it affects the behaviour of the engine at increasingly higher temperatures.

The importance to accurately account for impurities in an experimental environment is clearly demonstrated from the results. For asymmetric perturbations, the insertion positions that yield non-zero W_{tot}/T are displaced. This behaviour can again be explained by the energy level degeneracies of the system, as discussed in chapter 4. Since a displaced impurity affects the systems to the left and right of the well differently, the two-boson QSZE is no longer degenerate for a central insertion position.

Another observation that can be made is that a larger impurity affects the high temperature behaviour more than a small one. This is because a large perturbation can affect states with higher energies, which are only relevant at higher temperatures.

By comparing the two top figures in Fig. 5.1, we see that when a central impurity is added to the system, the system is less sensitive to variations in the insertion position in order to have non-zero W_{tot}/T. As discussed in chapter 4, we only see non-zero W_{tot}/T in the $T \to 0$ limit when the single-particle ground states $\varepsilon_1^{(L/R)}$ of the left and right subsystems are equal. Quantitatively speaking for low but finite temperatures, this condition relaxes to $|\varepsilon_1^{(L)} - \varepsilon_1^{(R)}| \ll k_B T$ due to the exponential terms of the partition function. The energy difference of the left and right ground states for a system without an impurity and for a system with a central impurity can be seen in Fig. 5.3. Here it is demonstrated that the system with an impurity is closer to degeneracy than the system without one which explains why it is less sensitive to insertion position.

Even though the insertion position is required to be less accurate in order to get non-zero W_{tot}/T, this is only the case for an impurity very close to the center. As can be seen in the figure third from the top in Fig. 5.1, a small displacement of the impurity can change the low temperature behaviour drastically. The need to be precise has not been removed but rather transferred from the insertion position to the position of the impurity. Nonetheless, perhaps this knowledge about the central impurity can be used to create a QSZE which is less sensitive to the insertion position of the barrier.

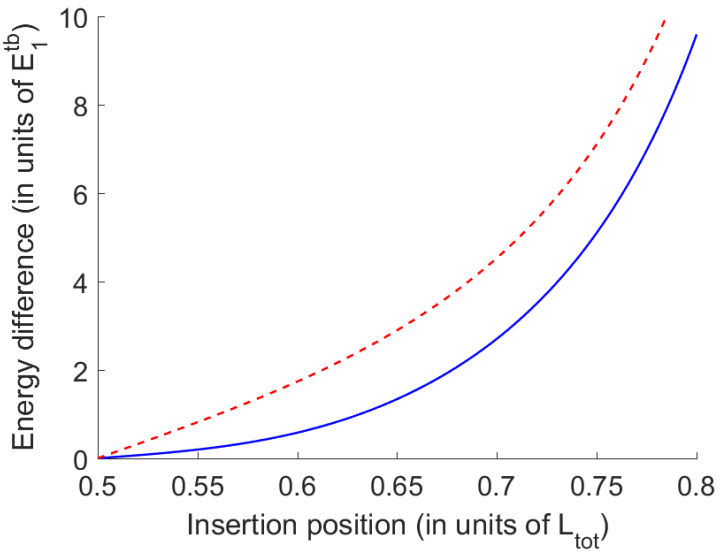

Figure 5.3: Energy difference between the ground states of the left and right subsystems $|\varepsilon_1^{(L)} - \varepsilon_1^{(R)}|$ for the two-boson QSZE as a function of barrier insertion position. *Blue solid line:* QSZE with a central impurity. *Red dashed line:* QSZE without an impurity. The results show that the system with an impurity has a lower difference between the energies of the ground states, *i.e.* it is closer to degeneracy than the system without an impurity.

Chapter 6

Dynamics

So far, the different steps of the Szilard engine have been assumed to be quasi-static and isothermal. This is of course an idealization, and in practice these requirements may not be reasonable. Even though modelling a system's interactions with a heat bath is outside the scope of this thesis, it can still be interesting to see what happens for some finite-time processes of the Szilard engine.

In this section I will first briefly review some theory and then study a single particle in an infinite well. I want to see what happens during the insertion and expansion processes of a Szilard engine that does not interact with a heat bath (which can be considered an approximation of an engine that is weakly coupled to its heat bath).

6.1 Theory

The time-evolution of a quantum system is described by the time-dependent Schrödinger equation

$$i\hbar\frac{d}{dt}\left|\Psi(t)\right\rangle = \hat{H}(t)\left|\Psi(t)\right\rangle . \tag{6.1}$$

A standard way of treating time-dependent systems is to expand the states in some time-independent basis $\{|\Phi_\nu\rangle\}$ and transfer all the time-dependence to the expansion-coefficients [29] according to

$$\left|\Psi(t)\right\rangle = \sum_{\nu=1}^{d} c_\nu(t)\left|\Phi_\nu\right\rangle , \tag{6.2}$$

where d is the size of the basis. By combining (6.1) and (6.2) and projecting onto the basis states $\{|\Phi_\nu\rangle\}$, we get the matrix equation

$$i\hbar \begin{pmatrix} \dot{c}_1 \\ \dot{c}_2 \\ \vdots \end{pmatrix} = \begin{pmatrix} \langle\Phi_1|\,\hat{H}(t)\,|\Phi_1\rangle & \langle\Phi_1|\,\hat{H}(t)\,|\Phi_2\rangle & \cdots \\ \langle\Phi_2|\,\hat{H}(t)\,|\Phi_1\rangle & \langle\Phi_2|\,\hat{H}(t)\,|\Phi_2\rangle & \cdots \\ \vdots & \vdots & \ddots \end{pmatrix} \begin{pmatrix} c_1 \\ c_2 \\ \vdots \end{pmatrix} \tag{6.3}$$

which is a system of ordinary differential equations that can be solved numerically in many different ways. Since the energies corresponding to the basis states used in Eq. (6.3) can be of very different size, this differential equation may be stiff [29], which means explicit numerical methods are typically unstable. With simplified notation, Eq. (6.3) can be rewritten as

$$\dot{\mathbf{c}}(t) = -\frac{i}{\hbar}\mathbf{H}(t)\mathbf{c}(t). \tag{6.4}$$

The pre-existing code that I have used propagates the system in time with a second order exponential propagator (see Refs. [30, 31] for a mathematical treatment of the exponential propagator) which enforces unitarity on the coefficients $\mathbf{c}$ to make the solutions numerically stable. This propagator has the form:

$$\mathbf{c}(t+\Delta t) = e^{-\frac{i}{\hbar}\Delta t\mathbf{H}(t+\frac{\Delta t}{2})}\mathbf{c}(t) + \mathcal{O}(\Delta t^3), \tag{6.5}$$

where $\mathcal{O}(\Delta t^3)$ are all terms of order three or higher in Δt. The size of the basis $\{|\Phi_\nu\rangle\}$ is often very large, which makes the exponential matrix in (6.5) expensive to calculate at every time step. To make the problem computationally less expensive, the matrix exponential is calculated within a Krylov space. The Krylov space is spanned by the vectors [31]

$$\{\mathbf{c}, \mathbf{Hc}, \ldots, \mathbf{H}^{m-1}\mathbf{c}\}, \tag{6.6}$$

where m is its dimension. A set of orthogonal vectors can, for instance, be obtained by applying the Gram-Schmidt method so that we get $\{\mathbf{k}_0, \mathbf{k}_1, \ldots, \mathbf{k}_{m-1}\}$ such that $\mathbf{k}_0 = \mathbf{c}$ and $\mathbf{k}_1$ is the part of $\mathbf{Hc}$ that is orthogonal to $\mathbf{k}_0$ and so forth.

We can, for some fixed n, write a single coefficient from (6.5) according to (omitting all terms of order higher than two)

$$c_n(t+\Delta t) = \sum_{\nu=1}^{d} \langle\Phi_n|\, e^{-\frac{i}{\hbar}\Delta t\hat{H}(t+\frac{\Delta t}{2})}\,|\Phi_\nu\rangle\, c_\nu. \tag{6.7}$$

If we now define abstract Krylov states $\{|k_i\rangle\}$ such that

$$\mathbf{k}_i = \begin{pmatrix} \langle \Phi_1 | k_i \rangle \\ \langle \Phi_2 | k_i \rangle \\ \vdots \end{pmatrix}, \tag{6.8}$$

we can insert these states into (6.7) so that

$$c_n(t + \Delta t) \approx \sum_{\nu=1}^{d} \sum_{i,j=1}^{m} \langle \Phi_n | k_i \rangle \langle k_i | e^{-\frac{i}{\hbar}\Delta t \hat{H}(t+\frac{\Delta t}{2})} | k_j \rangle \langle k_j | \Phi_\nu \rangle c_\nu. \tag{6.9}$$

Typically the dimension of the Krylov space is much smaller than the size of the many-body basis, which is why this method may help reduce the numerical effort. For example, it was found in Ref. [29] that a Krylov dimension of 30 could yield good results, while the many-body basis can have many thousand elements. Furthermore, the elements $\langle \Phi_n | k_i \rangle$ and $\langle k_i | e^{-\frac{i}{\hbar}\Delta t \hat{H}(t+\frac{\Delta t}{2})} | k_j \rangle$ can be constructed efficiently by using the Lanczos algorithm.

The reason the Krylov method can give good results even though the exponential matrix is calculated in a basis of significantly smaller size can be seen by expanding the exponential propagator in a power series (here omitting the argument of the Hamiltonian to simplify the notation)

$$\mathbf{c}(t + \Delta t) = e^{-\frac{i}{\hbar}\Delta t \hat{H}} \mathbf{c}(t) = \sum_{k=0}^{\infty} \frac{1}{k!} \left(-\frac{i}{\hbar} \Delta t \hat{H} \right)^k \mathbf{c}(t). \tag{6.10}$$

By expanding the sum and using (6.7) and (6.8), we get

$$\mathbf{c}(t + \Delta t) = \mathbf{c}(t) - \frac{i}{\hbar} \Delta t \hat{H} \mathbf{c}(t) - \frac{1}{\hbar^2} \Delta t^2 \hat{H}^2 \mathbf{c}(t) + \cdots \tag{6.11}$$

We can see that the vectors (6.6) used to construct the Krylov vectors act as a natural basis for the time-propagated coefficients. The reason that the expression (6.11) is not used explicitly is that the truncation of this expression is non-unitary. In order for the truncation of $\mathbf{c}(t + \Delta t)$ to have an absolute value close to one, the omitted higher order terms have to go to zero, which can be achieved by using a very small time step Δt but becomes computationally expensive.

6.2 Insertion

In previous chapters, the insertion process of the Szilard engine has been considered in a way such that the system is always able to adjust to the changes and maintain

a constant well-defined temperature. Here I will instead consider a barrier modelled by a delta function that increases in height at a constant rate until it reaches some maximal value for a system not coupled to a heat bath. I have chosen this maximal barrier height to be $20 \times 100\hbar^2/(L_{\text{tot}}^2 M)$ for all calculations in this section, which is a very high barrier compared to the lowest-lying states, *cf.* Fig. 4.3. This large value for the barrier height ensures that we at low temperatures have a system which, after insertion, behaves similarly to two infinite wells. I will study both a central and displaced insertion, where I have chosen the insertion point for the displaced barrier to be $L_{\text{tot}}/5$ from the center of the system.

As discussed in section 6.1, the state propagating in time is expanded in a basis such that all time-dependence is transferred to the expansion coefficients. For the insertion process, the state can be expanded in a basis corresponding to either the initial or final system according to

$$|\Psi(t)\rangle = \sum_{\nu=1}^{d} \tilde{c}_\nu(t)\,|\Phi_\nu^f\rangle = \sum_{\nu=1}^{d} c_\nu(t)\,|\Phi_\nu^i\rangle \tag{6.12}$$

The states $\{|\Phi_\nu^i\rangle\}$ correspond to the infinite well without any barrier, and $\{|\Phi_\nu^f\rangle\}$ to the final system, here the infinite well where the barrier has been fully inserted (either displaced or in the center).

The systems considered here have been initialized in one of the four lowest states of the initial system which is just the infinite well. The height of the delta barrier is then gradually increased at a constant speed until it reaches its maximal value. The propagating state is after insertion expressed in the basis of the final system. Results for a central and displaced barrier insertion are shown in Fig. 6.1.

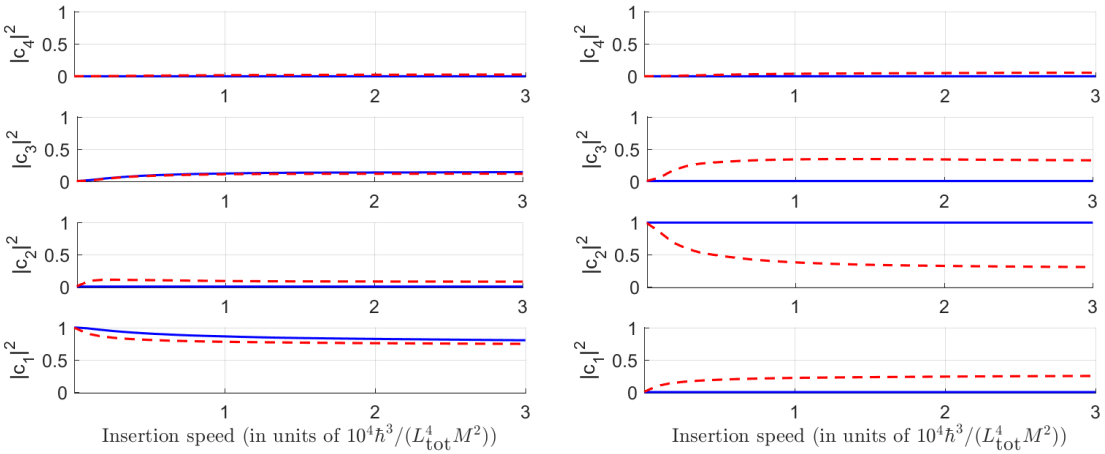

(a) $|\Psi(0)\rangle = |\Phi_1^i\rangle$

(b) $|\Psi(0)\rangle = |\Phi_2^i\rangle$

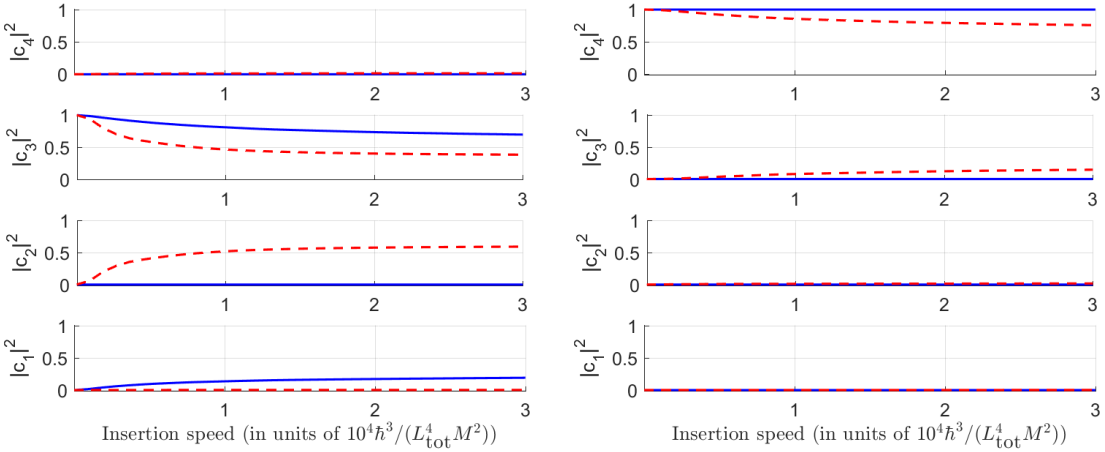

(c) $|\Psi(0)\rangle = |\Phi_3^i\rangle$

(d) $|\Psi(0)\rangle = |\Phi_4^i\rangle$

Figure 6.1: Populations of the four lowest states just as the insertion process is complete as a function of insertion speed. The state is expanded in states of the final system. *Blue solid line:* Central barrier. *Red dashed line:* Displaced barrier. It can be seen that the displaced insertion reaches the adiabatic limit more slowly than the central one.

The results show that for a central barrier insertion, only systems initialized to odd-numbered states are subject to excitations. This is because all even-numbered states of the initial system have a node in the center of the well, which leaves them unaffected by the infinitely thin delta-barrier. Another thing that can be seen is

that the states initialized to an odd-numbered state only have excitations to other odd-numbered states. This is due to parity being good quantum number when the barrier is perfectly central. For the displaced barrier we see no such effects since parity is no longer good quantum number. We may from these results also conclude that the insertion needs to be slower for the displaced barrier than for the central one in order to reach the adiabatic limit, *i.e.* when there are no excitations.

The excitations due to a finite insertion speed will affect the work cost of the insertion process. I will denote the energies of the initial system by E_j and final system by $\tilde{E}_i$. For a system initialized to the jth state there must be an average work cost $\langle W_j \rangle$ of

$$\langle W_j \rangle = \left(\sum_i |\tilde{c}_i^j|^2 \tilde{E}_i \right) - E_j \tag{6.13}$$

associated with the insertion process. Here $\tilde{c}_i^j$ are the expansion coefficients of the state after insertion in the final system, when the system is initialized to the jth state. If we assume the initial system to be canonically distributed, the total average work cost $\langle W_{\text{tot}} \rangle$ of the insertion process becomes

$$\langle W_{\text{tot}} \rangle = \frac{1}{Z} \sum_j e^{-\beta E_j} \langle W_j \rangle = \frac{1}{Z} \sum_j e^{-\beta E_j} \left[\left(\sum_i |\tilde{c}_i^j|^2 \tilde{E}_i \right) - E_j \right]. \tag{6.14}$$

where $Z = \sum_j e^{-\beta E_j}$ is the partition function.

The total average work cost of the insertion process as a function of insertion speed can be seen in Fig. 6.2. Here, each set of data is expressed in units of the corresponding work cost for an isothermal and quasi-static process according to (2.20). From these results we can conclude that an insertion at finite speed costs more work than a quasi-static and isothermal insertion, and that the work cost increases rapidly with increasing insertion speeds. Another observation that can be made is that the work cost for insertion compared to the isothermal and quasi-static case is much higher for the displaced barrier than for the central at low temperatures. As demonstrated by Fig. 6.2, the work cost at low temperatures for an isothermal and quasi-static insertion is lower for a displaced barrier than for a central one. This lower work-cost is lost when we account for finite-speed effects, which means that a QSZE which has its optimal work output for non-central insertions—such as, for example, a QSZE with an even number of fermions—loses more work output than a QSZE with optimum for central insertions.

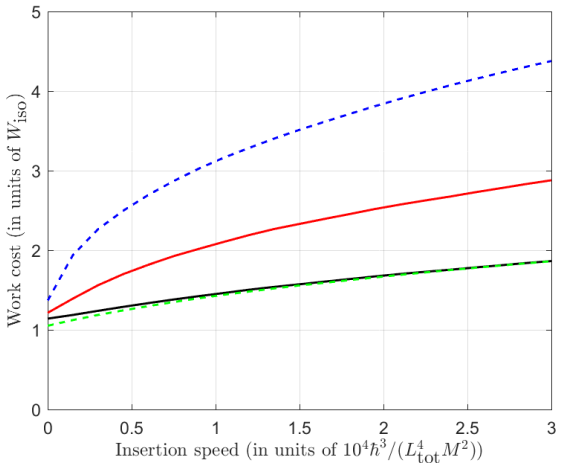

Figure 6.2: Work cost for inserting a barrier as a function of insertion speed. The work cost is given in units of W_{iso}, the work cost of inserting the barrier isothermally and quasi-statically according to (2.20) (*i.e.* different values of W_{iso} for each line). Here E_1 is the energy of the ground state of the unperturbed system. *Red solid line:* central barrier at $T = E_1/k_B$. *Blue dashed line:* displaced barrier at $T = E_1/k_B$. *Black solid line:* central barrier at $T = 10E_1/k_B$. *Green dashed line:* displaced barrier at $T = 10E_1/k_B$.

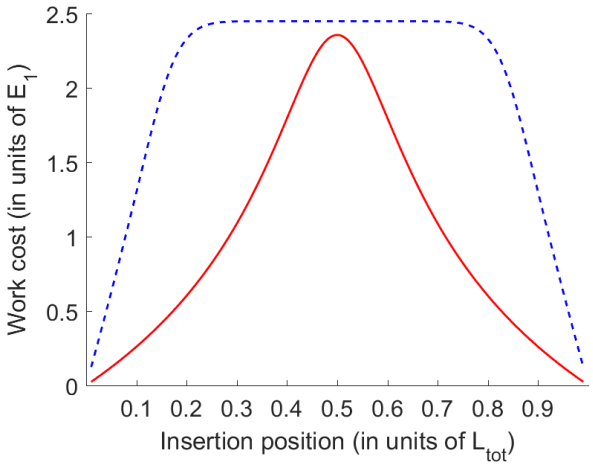

Figure 6.3: Work cost for inserting a barrier isothermally and quasi-statically according to (2.20) as a function of barrier insertion position for a QSZE with one particle. *Red solid line:* T $= E_1/k_B$. *Blue dashed line:* $10E_1/k_B$.

6.3 Expansion

The expansion process here is modelled by an infinite well with one moving wall that moves at a constant speed until it reaches some maximal value and then stops. Just as for the insertion process, the states are initialized to some state of the initial system, here an infinite well of half the width of the final system. The well is then expanded, and the propagating state is expanded in this new system. Figure 6.4 shows results for the populations after the expansion has been completed.

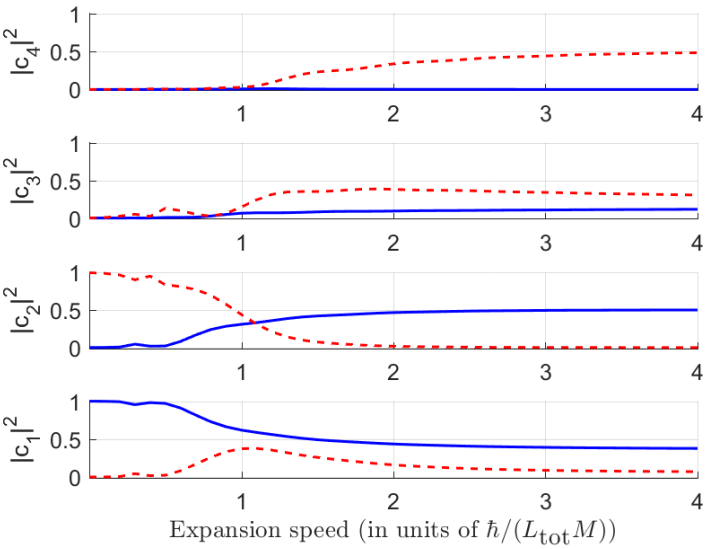

Figure 6.4: Populations of the four lowest states just as the expansion process is complete as a function of expansion speed. The state is expanded in states of the final system. *Blue solid line:* $|\Psi(0)\rangle = |\Phi_1^i\rangle$. *Red dashed line:* $|\Psi(0)\rangle = |\Phi_2^i\rangle$.

We can see from the results that the adiabatic limit is once again obtained as the expansion speed becomes very slow. For an instantaneous expansion, the expansion coefficients of the final system can be obtained analytically. Both the initial and final systems are infinite wells, which have the wave functions [19]

$$\psi_n(x) = \sqrt{\frac{2}{L}} \sin\left(\frac{n\pi x}{L}\right) \tag{6.15}$$

for a well of length L. Here the initial width of the system is $L_i = L_{\mathrm{tot}}/2$ and the final $L_f = L_{\mathrm{tot}}$, where L_{tot} is the total length of the system. The initial wave function

$\psi_{L_i,m}$ can be expressed in wave functions $\psi_{L_f,m}$ of the final system

$$\psi_{L_i,m}(x) = \sum_n c_n^m \psi_{L_f,n}(x). \tag{6.16}$$

Orthogonality of the wave functions gives, for a system initialized to the mth state, the expansion coefficients c_n^m as

$$c_n^m = \frac{2}{\sqrt{L_i L_f}} \int_0^{L_i} \sin\left(\frac{m\pi x}{L_i}\right) \sin\left(\frac{n\pi x}{L_f}\right) dx. \tag{6.17}$$

Evaluating the integral gives

$$\begin{aligned}
|c_1^1|^2 &= \frac{32}{9\pi^2} \approx 0.36 \\
|c_2^1|^2 &= \frac{1}{2} \\
|c_3^1|^2 &= \frac{32}{25\pi^2} \approx 0.13 \\
|c_4^1|^2 &= 0
\end{aligned}$$

for a system initially in the ground state and

$$\begin{aligned}
|c_1^2|^2 &= \frac{128}{225\pi^2} \approx 0.058 \\
|c_2^2|^2 &= 0 \\
|c_3^2|^2 &= \frac{128}{49\pi^2} \approx 0.26 \\
|c_4^2|^2 &= \frac{1}{2}
\end{aligned}$$

for a system initially in the first excited state, which is in good agreement with the results in Fig. 6.4.

Results for how the probability distribution changes in time for a system which is initially in the ground state of the initial system is shown in Fig. 6.5. For a slow expansion, the probability distribution constantly becomes the probability distribution of the ground state in the new expanded well, but with some oscillations due to the finite expansion speed. For the fast expansion, the wave function of the system does not have time to adjust, and the particle's probability distribution oscillates between the two halves of the well. This property is of interest for a Szilard engine

working continuously as the position of the particle will be known before insertion and thus before measurement. If the position is known beforehand no information can be extracted and the engine can not perform any work.

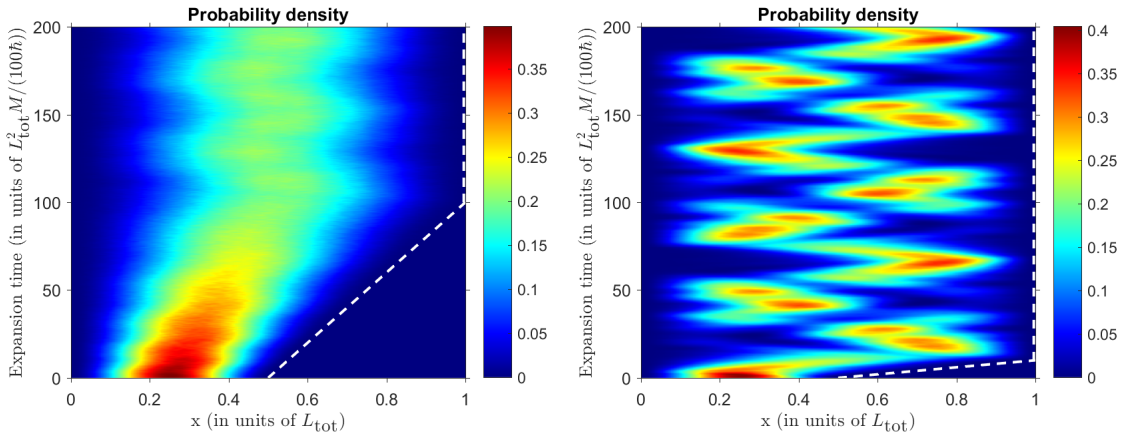

(a) (b)

Figure 6.5: Probability distributions for a system initialized to the ground state of the initial system as a function of space and time. One of the infinite well's walls is at all times at $x = 0$ while the other is marked by the dashed white line. **(a)** Slow expansion, $v_{\mathrm{exp}} = 0.5 \times \hbar/(L_{\mathrm{tot}}M)))$. **(b)** Fast expansion, $v_{\mathrm{exp}} = 5.0 \times \hbar/(L_{\mathrm{tot}}M)))$

Chapter 7

Conclusions and Outlook

I have in this project studied a few aspects of the quantum Szilard engine that have not received much attention previously. The work I have done is mainly numerical, applying the configuration interaction method, complemented by a few analytical considerations.

In chapter 4 the contact-interaction was studied for bosons with a focus on maximizing the work output of the QSZE. The contact-interaction was used here mainly because of it being easy to incorporate into the model. Despite this, interactions that can be described by a contact-interaction appear experimentally in cold atoms [24]. Quasi one-dimensional systems of cold atoms can be achieved by exposing a system to strong two-dimensional optical lattices [24]. In these types of systems the interaction strength depends on the scattering length, which can be controlled by external magnetic fields via Feshbach resonances [32]. The tunability of the interaction strength suggests cold atoms as one interesting way to realize a quantum Szilard engine. A big problem with this approach is the heat bath. It is unclear how to implement a constant temperature heat bath for a system of cold atoms. Additionally, a very cold system would likely have to work very slowly to fit the isothermal and quasi-static approximations. Here a complete dynamical study of the interactions between a QSZE and its heat bath could be of interest. It should also be mentioned that the confining potential for optical lattices is not an infinite well [33], as has been the case throughout this thesis. To study the effect that different confining potentials have on the Szilard engine is one way to continue the work of this thesis.

An unanswered question from chapter 4 of this thesis is whether the work output of the QSZE with contact-interacting bosons keeps increasing with particle number and, if that is the case, in what way and how much. A hint of this behaviour could be obtained by studying a QSZE with four or perhaps five particles in the same manner

as in this thesis. This would require very lengthy computations but could still be feasible.

While I have looked mostly at the average work output of a single cycle of the QSZE, a better measure of an engine's usefulness is its power. How the insertion, expansion and removal steps of the engine should be carried out in order to maximize the engine's power is an interesting question. To properly examine these aspects a full dynamical study, with a model to properly account for the engine's interactions with a heat bath, would have to be made.

Bibliography

[1] L. Szilard, *Z. Phys.* **53**, 840 (1929) (english translation reprinted in [2])

[2] H. S. Leff and A. F. Rex, *Maxwell's Demon 2: Entropy, Classical and Quantum Information, Computing* (IOP Publishing, Bristol, 2003)

[3] W. Zurek, e-print: arXiv:quant-ph/0301076 (1984) (originally printed in *Frontiers of Nonequilibrium Statistical Physics*, Plenum Press, New York)

[4] S. W. Kim, T. Sagawa, S. De Liberato, and M. Ueda, *Phys. Rev. Lett.* **106**, 070401 (2011)

[5] K. H. Kim and S. W. Kim, *Phys. Rev.* E **84**, 012101 (2011)

[6] K. H. Kim and S. W. Kim, e-print: arXiv:1108.3644v3 (2011)

[7] C. Y. Cai, H. Dong, and C. P. Sun, *Phys. Rev.* E 85, 031114 (2012)

[8] M. Plesch, O. Dahlsten, J. Goold, and V. Vedral, *Scientific Reports* **4**, 6995 (2014)

[9] Z. Zhuang and S. D. Liang, *Phys. Rev.* E **90**, 052117 (2014)

[10] H. J. Jeon and S. W. Kim, *New. J. Phys.* **18**, 043002 (2016)

[11] S. Toyabe, T. Sagawa, M. Ueda, E. Muneyuki, and M. Sano, *Nature Physics* **6**, 988 (2010)

[12] J. V. Koskia, V. F. Maisia, J. P, Pekola, and D. V. Averind, *Proc. Natl. Acad. Sci. USA* **111**, 13786 (2014)

[13] R. Landauer, *IBM J. Res. Dev.* **5**, 183 (1961)

[14] K. Maruyama, F. Nori, and V. Vedral, *Rev. Mod. Phys.* **81**, 1 (2009)

[15] C. H. Bennett, *Int. J. Theor. Phys.* **21**, 905 (1982)

[16] T. D. Kieu, *Phys. Rev. Lett.* **93**, 140403 (2004)

[17] M. Plesch, O. Dahlsten, J. Goold, and V. Vedral, *Phys. Rev. Lett.* **111**, 188901 (2013)

[18] S. W. Kim, T. Sagawa, S. De Liberato, and M. Ueda, *Phys. Rev. Lett.* **111**, 188902 (2013)

[19] J. J. Sakurai and J. J. Napolitano, *Modern Quantum Mechanics, Second Edition* (Pearson Education Limited, Harlow, 2010)

[20] E. K. U. Gross, E. Runge, and O. Heinonen, *Many-Particle Theory* (IOP Publishing, Bristol, 1991)

[21] A. L. Fetter and J. D. Walecka, *Quantum Theory of Many Particle Systems* (Dover Publications, Mineola, New York, 2003)

[22] The LAPACK library, http://www.netlib.org/lapack/

[23] G. H. Golub and C. F. van Loan, *Matrix Computations, Third Edition* (The John Hopkins University Press, Baltimore and London, 1996)

[24] I. Bloch, J. Dalibard, and W. Zwerger *Rev. Mod. Phys.* **80** 885 (2008)

[25] C. de Boor, *A Practical Guide to Splines* (Springer-Verlag, New York, 1978)

[26] D. G. Anderson, *Math. Comp.* **19**, 477 (1965)

[27] K. Huang, *Statistical Mechanics* (John Wiley & Sons, 1963)

[28] M. Girardeau, *J. Math. Phys.* **1**, 516 (1960)

[29] J. C. Cremon, e-print: arXiv:1301.7596v1 (2013)

[30] M. Hochbruck and C. Lubich, *SIAM J. Numer. Anal.* **34**, 1911 (1997)

[31] Y. Saad, *SIAM J. Numer. Anal.* **29**, 209 (1992)

[32] C. Chin, R. Grimm, P. Julienne, and E. Tiesinga, *Rev. Mod. Phys.* **82** 1225 (2009)

[33] I. Bloch, *Nature Physics* **1**, 23 (2005)